Dalton Transactions

PAPER

View Article Online
View Journal | View Issue



Cite this: *Dalton Trans.*, 2014, **43**, 12590

# 1,3,5,7-Tetrakis(tetrazol-5-yl)-adamantane: the smallest tetrahedral tetrazole-functionalized ligand and its complexes formed by reaction with anhydrous M(II)$Cl_2$ (M = Mn, Cu, Zn, Cd)†‡

Ishtvan Boldog,*[a,b] Konstantin V. Domasevitch,[b] Joaquín Sanchiz,[c] Peter Mayer[d] and Christoph Janiak*[a]

Received 6th April 2014,
Accepted 23rd June 2014

DOI: 10.1039/c4dt01022a

www.rsc.org/dalton

1,3,5,7-Tetrakis(tetrazol-5-yl)-adamantane ($H_4L$) was probed as a building block for the synthesis of tetrazolato/halido coordination polymers with open-network structures. $MCl_2$ (M = Cu, Cd, Zn, Mn) was reacted with $H_4L$ in DMF at 70 °C to yield $[Cu_4Cl_4L(DMF)_5]\cdot DMF$, **1**; $[Cd_4Cl_4L(DMF)_7]\cdot DMF$, **2**; $[Zn_3Cl_2L(DMF)_4]\cdot 2DMF$, **3** and $[Mn_2L(DMF)_2(MeOH)_4]\cdot DMF\cdot 2MeOH\cdot 2H_2O$, **4**. **1** and **2** (*Fddd*) are nearly isostructural and have zeolitic structures with a $\{4^3\cdot 6^2\cdot 8\}$, **gis** or gismondine underlying net, where the role of the tetrahedral nodes is served by the coordination bonded clusters and the adamantane moiety. **3** ($P2_1/n$) has a porous structure composed of coordination bonded layers with a $(4\cdot 8^2)$ **fes** topology joined *via trans*-{Zn(tetrazolate)$_2$(DMF)$_4$} pillars with an overall topology of $\{4\cdot 6^2\}\{4\cdot 6^6\cdot 8^3\}$, **fsc**-3,5-*Cmce*-2. **4** ($Pca2_1$) is composed of stacked $\{Mn_2L\}$ hexagonal networks. In **1** and **2** the ligand fulfills a symmetric role of a tetrahedral building block, while in **3** and **4** it fulfills rather a role of an effective trigonal unit. Methanol-exchanged and activated **1** displayed an unusual type IV isotherm with H2 type hysteresis for $N_2$ sorption with an expected uptake at high $P/P_0$, but with a smaller $S_{BET}$ = 505.5 $m^2\ g^{-1}$ compared to the calculated 1789 $m^2\ g^{-1}$, which is a possible result of the framework's flexibility. For $H_2$ sorption 0.79 wt% (1 bar, 77 K) and 0.06 wt% (1 bar, RT) uptake and $Q_{st}$ = −7.2 kJ $mol^{-1}$ heat of adsorption (77 K) were recorded. Weak antiferromagnetic interactions were found in **1** and **4** with $J_1$ = −9.60(1), $J_2$ = −17.2(2), $J_3$ = −2.28(10) $cm^{-1}$ and $J$ = −0.76 $cm^{-1}$ respectively. The formation of zeolitic structures in **1** and **2**, the concept of structural 'imprinting' of rigid building blocks, and design opportunities suggested **4** as a potential hexafunctionalized biadamantane building block.

## Introduction

Polyfunctional tetrazolate ligands are receiving significant attention as building blocks[1] for the synthesis of porous coordination polymers (PCPs/MOFs).[2] These materials characterized by outstanding surface areas are potentially interesting for a number of applications.[3] High number of donor sites allows the tetrazolate to be involved in large, densely interconnected polynuclear clusters, which are robust building blocks (SBUs) for support of framework solids and possible functional entities in the context of magnetism or luminescence.[1] Large clusters disfavour interpenetration, which is an advantage for enhancement of porosity related parameters, and providing potential coordinatively unsaturated metal centers (UMCs) ensures enhanced sorptive capabilities.[4] UMCs formed by removal of the coordinated solvent molecules are characterized by increased affinity to a wide range of substrates, giving rise to enhanced and selective physisorption of gases[5] and coordinatively mediated catalysis.[6]

The high number of donor functions endows the tetrazolate function with a capability to sustain unusually high number of coordination bonded arrangements (patterns)[7] compared to other azolates. In the case of simple rigid ligands it is a prerequisite for assembly of a highly symmetric framework, with a

[a]*Institut für Anorganische Chemie und Strukturchemie, Universität Düsseldorf, Universitätsstr. 1, D-40225 Düsseldorf, Germany. E-mail: ishtvan.boldog@gmail.com*
[b]*Inorganic Chemistry Department, Taras Shevchenko National University of Kiev, Vladimirskaya Street 64, Kiev 01033, Ukraine*
[c]*Departamento de Química Inorgánica, Universidad de La Laguna, c/o Astrofísico Francísco Sánchez s/n, 38206 La Laguna, Tenerife, Spain*
[d]*Department Chemie, Ludwig-Maximilians-Universität München, Butenandtstr. 5-13, Haus D, D-81377 München, Germany*

† Dedicated to Prof. Marius Andruh on the occasion of his 60th birthday.

‡ Electronic supplementary information (ESI) available: Additional notes and information concerning single crystal XRD structure determination and analytics, including NMR, TGA, PXRD, IR and sorption analyses. CCDC 991447–991450. For ESI and crystallographic data in CIF or other electronic format see DOI: 10.1039/c4dt01022a

significant probability of isomerism. Indeed, the linear 1,4-benzeneditetrazole ($H_2BDT$)[8] and flat triangular 1,3,5-benzenetristetrazole ($H_3BTT$)[9] were successfully used for the synthesis of a number of notable PCPs with robust and symmetric structures. Among the results is the consistent reproduction of sodalite frameworks and the achievement of a near-record $H_2$ heat of sorption value at 10.5 kJ $mol^{-1}$ for one of them in $\{Co_3[(Mn_4Cl)_3(BTT)_8]_2 \cdot 1.7CoCl_2\}$.[9]

Our interest is focused on PCPs based on 'tetrahedral' ligands, *i.e.* tetrafunctionalized rigid tetrahedral platforms, which are in general less investigated compared to their planar counterparts. Once researched actively, with notable results using tetrahedral carboxylate,[10] phosphonate,[11] and sulfonate ligands,[12,13] this direction of research temporarily declined, seemingly due to the perception that tetrahedral platforms yield too dense or interpenetrated structures. Recently there have been signs of revival of the area, partly due to recognition of the fact that the use of massive coordination-bonded clusters as secondary building units (SBU) of high connectedness could be efficient.[14,15] Notable examples are coordination polymers with the fluorite structure, based on eight-connected SBUs, which are found either for tetrazolates[16–18] and recently for carboxylate building blocks.[19] To the best of our knowledge there are five papers devoted to 'tetrahedral' azole/azolate ligands, namely tetrazole[16–18,20] and triazole[21] functionalized ones. Two manganese compounds,[16,20] based on similar 'tetrahedral' tetrazolates and involving chloride anions as co-ligands, serve as an interesting example of variability of coordination-bonded cluster geometry and size due to involvement of short halido bridges.[16,20] It was conjectured that mixed tetrazolato/halido coordination polymers constitute an interesting compound class with 'scalable' multinuclear clusters,[20] which are interesting either as robust SBUs or possibly as functional magnetic units.

In this contribution we probed the practically unexplored 1,3,5,7-tetrakis(tetrazol-5yl)adamantane ligand ($H_4L$) as a building block for coordination polymers using conditions favoring formation of tetrazolato/halido clusters (Scheme 1). This ligand in anionic form has one of the highest density of donor sites achievable for a 'tetrahedral' ligand, which is a prerequisite for rich coordination and structural chemistry of derived coordination-bonded frameworks.

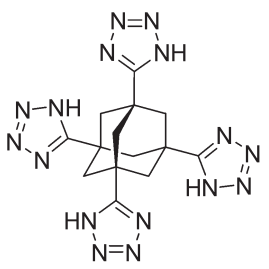


$H_4L$

Scheme 1 1,3,5,7-Tetrakis(tetrazol-5-yl)adamantane.

## Results and discussion

### The ligand

Universal rigid molecular platforms with tetrahedral symmetry are typically limited to tetraphenylmethane (including 9,9′-spirobifluorene) and adamantane, as well as their phenyl augmented and heteroatom-substituted analogues.[14] Adamantane is the smallest tetrahedral platform next only to quaternary carbon, while the latter has inherent steric limitations. Adamantane is widely used for the synthesis of organic polymers (recently with an emphasis on porous organic polymers and covalent organic frameworks),[22] dendrimers,[23] and molecular entities for supramolecular synthesis[24] and nanotechnology.[25] Compared to tetraphenylmethane, whose modification is standard and facile, the chemistry of adamantanes is peculiar, at times cumbersome, but offering synthetic opportunities as well. For example adamantane could be selectively brominated in bridgehead positions to afford mono- to tetra-substituted adamantanes in high yields.[26] However, 1,3,5,7-tetrabromoadamantane is the most chemically inert entity in the row and the substitution of halogens *via* the $S_{N1}$ mechanism demands harsh conditions. It was not only until the recent paper of Lee *et al.*,[27] in which photochemical cyanodebromination of 1,3,5,7-tetrabromoadamantane was described that a facile route to various tetrasubstituted adamantanes, including the fundamental 1,3,5,7-tetracarboxyadamantane, became available.

'Click chemistry' of tetrazole formation,[28,29] by cycloaddition of azides to nitriles in the presence of $ZnCl_2$ makes the tetrakis-tetrazole derivative of adamantane especially affordable (Scheme 2). 1,3,5,7-Tetracyanoadamantane reacts somewhat slower than the aromatic- or non-hindered aliphatic nitriles, yielding the 1,3,5,7-tetrakis(tetrazol-5-yl)adamantane, $H_4L$. The process works satisfactorily in DMF under reflux for 48 h or at 175 °C in an autoclave within 6 hours (the first condition provides a purer product). If shorter times are used (12–24 h) the

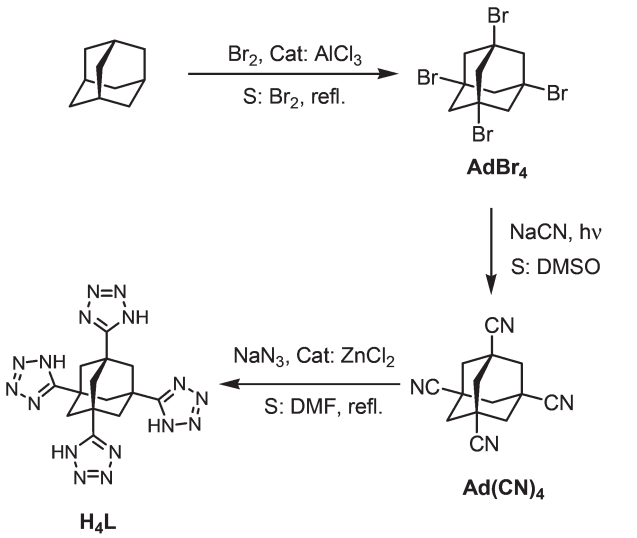


Scheme 2 Synthesis of $H_4L$ starting from adamantane.

reaction is mostly completed, but minor amounts of semi-converted intermediary compounds complicate the purification.

$H_4L$ is an acid and its alkali metal and ammonia salts are well soluble in water. Their formation was used for purification. Upon acidification of an alkaline solution, $H_4L{\cdot}3H_2O$ precipitates ($P2_1/n$, $a$ = 12.093 Å, $b$ = 10.314 Å, $c$ = 16.481 Å, $\beta$ = 108.6°), in which two out of three molecules of water are bound remarkably strongly, forming H-bonds with the tetrazolyl groups. Complete dehydration occurs only at approximately 190 °C (Fig. S1‡) and the anhydrous compound is hygroscopic (in this work the ligand was used in hydrated form; no difference except, possibly, variation of yield and crystallinity of the product were found between the use of anhydrous or hydrated ligands). $H_4L$ is very well soluble in highly polar solvents such as DMSO (also forms a stable crystalline solvate with two molecules of solvent; $H_4L{\cdot}4$DMSO, $I4_1/a$, $a = b$ = 16.8580, $c$ = 11.5483), DMF and slightly in acetic acid. It has low solubility in water, which rises remarkably with temperature, potentially allowing hydrothermal crystallizations of coordination polymers, and low solubility in medium- and non-polar solvents including alcohols.

To the best of our knowledge the first and only coordination compound of the $H_4L$ ligand was communicated by us recently.[18] The $\{[Cu_4(\mu_4\text{-}Cl)(L)_2]_2Cu\}{\cdot}9$DMF complex, a representative of a fluorite isoreticular series of networks with a 'crown-shaped' tetranuclear cluster demonstrated the similarity of the shortest representative of the tetrahedral ligand class to scaled-up analogs.[18] The unique donor atom density of $L^{4-}$ suggests rather differences than common behaviour with scaled-up analogues.

The free $H_4L$ ligand with a composition of $C_{14}H_{16}N_{16}$ rather reminds of a high-energetic molecule with possible explosive properties. Indeed it decomposes near-explosively at a temperature around 270 °C, but $L^{4-}$ is surprisingly stable as a constituent part of the compounds reported in this paper and is not sensitized by coordination, at least the thermal decomposition is smooth. The 'green primary explosives' based on 5-nitrotetrazolate complexes[30] are oxygen rich and have much higher nitrogen content, indicating that $H_4L$ should be much less sensitive.

**Structures of $[Cu_4Cl_4L(DMF)_5]{\cdot}$DMF, 1 and $[Cd_4Cl_4L(DMF)_7]{\cdot}$DMF, 2.** Crystallizations using $CuCl_2$ and $CdCl_2$ afforded the nearly isostructural compounds **1** and **2**. Four metal atoms are arranged in a zig-zag chain along the $z$-axis and joined by two $\mu_3$-tetrazolate-κN1:κN2:κN3, two $\mu_3$-tetrazolate-κN2:κN3 and three $\mu_2$-Cl bridging groups to constitute the structure defining coordination-bonded cluster, $\{M_4Cl_4(\text{tetrazolate})_4(DMF)_n\}$ (Fig. 1b and 4b).

The inner part of the tetranuclear cluster arrangement is represented by two equivalent *mer*-$\{MN_3Cl_2O\}$ octahedral ions. The outer ions, though crystallographically equivalent, should be viewed as chemically different. The crystallographic data clearly define the three bridging chlorides, but the electroneutrality of the compound demands the presence of a fourth chloride ion. Theoretically it could be located in the cavities of the structure, but the charge separation between the cationic framework and the anion is improbable, when there are a number of suitable coordination positions that could be filled. The diffraction experiment showed that the electronic densities are increased near the O-atoms of the coordinated solvent molecules and the most reasonable explanation is that they should be associated with the 'missing' chloride. The O- and Cl-atoms are positionally disordered (0.5 : 0.5 to 0.8 : 0.2 ratios) and thus the crystallographically equivalent terminal metal atoms in the cluster are a superimposition of square-pyramidal $\{CuN_2Cl_2O\}$ and $\{CuN_2ClO_2\}$ in the case of **1** (Addison $\tau$ parameter[34] is ~0.06) or two octahedral $\{CdN_2Cl_2O_2\}$ and *fac*-$\{CdN_2ClO_3\}$ metal centers in the case of **2**. The higher coordination number expressed by these atoms in **2** is the main difference between the nearly isostructural **1** and **2**, which is facilitated by slight expansion of the structure due to longer Cd–N and Cd–Cl compared to Cu–N and Cu–Cl bonds. The Cu–N and Cd–N bond lengths are fairly uniform: 1.99–2.04 Å for the former, except a single case of a very long Cu2–N5 bond, 2.466(5) Å, while the Cd–N distances do not demonstrate such a separation, residing in the 2.29–2.42 Å range (Table 1). The Cu–Cl bond lengths to bridging chlorides are strongly scattered, 2.283(2), 2.735(2) Å (Cl1) and 2 × 2.599(3) Å (Cl2), while the analogous Cd–Cl bonds again are more uniform, 2.583(3), 2.677(2) Å (Cl1) and 2 × 2.612(2) Å (Cl2), *i.e.* either it is an example of Jahn–Teller distortion in the case of **1** or the structure of **2** is less strained. In any case the presence of the unusual bond lengths in the cluster is a prerequisite for possible framework flexibility (bistability) in the case of **1**, possibly a cause of the unusual results of the adsorption measurements (see below).

It is also worth noting that the residual electronic density analysis for **2** suggests that the disorder of the chloride anion is possibly more complex and incorporates additional positions occupied by the DMF molecules; however, the occupation factors associated with them are relatively low. In the refined simplified model, the anion is disordered over two positions, which remain strictly unoccupied in **1** and correspond to the sub-basal part of the square-pyramidal environment of copper.

The $\{M_4Cl_4(\text{tetrazolate})_4(DMF)_n\}$ tetranuclear cluster with equal number of tetrazolate groups represents a four connected node from a topological point of view. Its geometry, though resembling a chain, with almost equal separations between the metal atoms (3.54–3.58 Å), could be compared to a strongly distorted tetrahedron (Fig. 1b). The halves of the tetranuclear cluster are related by a 2-fold axis, comparable with a similar relation between the halves of a regular tetrahedron; however, the level of distortion in the former case is very high. The ligand represents the second four-connected node with a perfect tetrahedral symmetry. The resulting underlying net corresponds to the topology of a uninodal **gis**, or gismondine net (point symbol: $\{4^3{\cdot}6^2{\cdot}8\}$, vertex symbol: $4{\cdot}4{\cdot}4{\cdot}8(2){\cdot}8{\cdot}8$)[60] (Fig. 1c and d), which is also observed in the eponymous zeolite. Thus, despite a metrical difference between the bonding directions supported by the nodes, the latter are topologically equivalent.

 

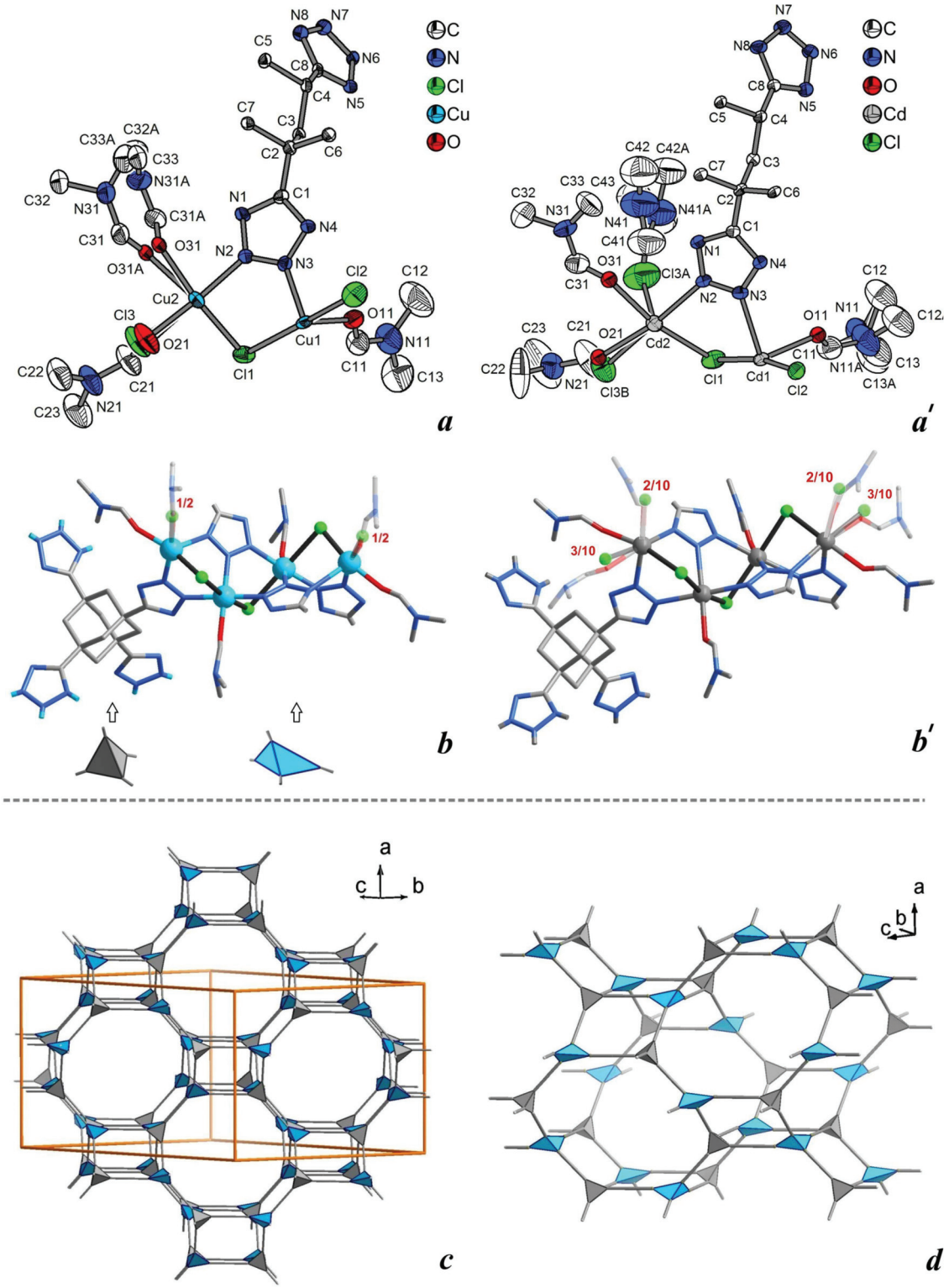


**Fig. 1** Structures of $[Cu_4Cl_4L(DMF)_5]\cdot DMF$, **1** and $[Cd_4Cl_4L(DMF)_7]$, DMF, **2**. (a) ORTEP drawing of the asymmetric unit at the 50% probability level. Minor components of the disordered DMF solvent molecules and the pore-filling DMF molecules are not shown for clarity. (b) Two tetrahedral units constituting the structure are given explicitly: the covalent adamantane-based moiety and the tetranuclear coordination-bonded cluster. The positionally disordered components of the solvent molecules are collapsed to one component, while the occupationally disordered moieties are given in half-transparent style and marked with a red index of the occupancy factor of the chloride anion. (c, d) Network representation of the structures on the example of **1** corresponding to a topology of gismondine.

**Table 1** M–N, M–O and M–Cl bond lengths (Å) and X–M–X angles (°), X = N, μ-Cl, for **1–4**. Angles involving non-bridging Cl atoms for **3** and O atoms for **4** are given additionally

| $[Cu_4Cl_4L(DMF)_5]\cdot DMF$, **1** | | $[Cd_4Cl_4L(DMF)_7]\cdot DMF$, **2** | | $[Zn_3Cl_2L(DMF)_4]\cdot 2DMF$, **3** | | $[Mn_2L(DMF)_2(MeOH)_4]\cdot DMF\cdot 2MeOH\cdot 2H_2O$, **4** | |
|---|---|---|---|---|---|---|---|
| Cu1–N3 | 1.990(5) | Cd2–N2 | 2.298(5) | Zn1–N1 | 2.010(4) | Mn1–N2 | 2.252(5) |
| Cu1–N6#b | 2.033(5) | Cd1–N3 | 2.292(4) | Zn2–N5 | 2.000(3) | Mn2–N3 | 2.239(4) |
| Cu1–N7#a | 2.002(5) | Cd2–N5#b | 2.416(4) | Zn1–N10#b | 2.042(4) | Mn2–N6#b | 2.230(5) |
| Cu2–N2 | 1.993(5) | Cd1–N6#b | 2.386(5) | Zn1–N14#c | 2.046(5) | Mn1–N7#b | 2.267(4) |
| Cu2–N5#b | 2.466(5) | Cd1–N7#a | 2.316(4) | Zn2–N11#b | 2.057(4) | Mn1–N10#a | 2.248(5) |
| Cu1–O11 | 1.978(5) | Cd1–Cl1 | 2.677(2) | Zn2–N15#c | 2.026(4) | Mn2–N11#a | 2.251(5) |
| Cu2–O21 | 1.919(16) | Cd1–Cl2 | 2.612(2) | Zn3–N3 | 2.163(5) | Mn1–O1 | 2.183(4) |
| Cu2–O31 | 2.033(9) | Cd2–Cl1 | 2.583(3) | Zn3–N7#e | 2.206(5) | Mn1–O2 | 2.161(6) |
| Cu2–O31A | 2.108(9) | Cd2–Cl3B | 2.464(19) | Zn3–O1 | 2.101(3) | Mn1–O3 | 2.159(6) |
| Cu1–Cl1 | 2.735(2) | Cd2–Cl3A | 2.588(15) | Zn3–O2 | 2.068(3) | Mn2–O4 | 2.135(6) |
| Cu1–Cl2 | 2.599(3) | Cd1–O11 | 2.301(4) | Zn3–O3 | 2.086(4) | Mn2–O5 | 2.176(4) |
| Cu2–Cl1 | 2.283(2) | Cd2–O21 | 2.250(12) | Zn3–O4 | 2.072(3) | Mn2–O6 | 2.174(4) |
| Cu2–Cl3 | 2.213(6) | Cd2–O31 | 2.298(5) | Zn1–Cl1 | 2.1861(13) | | |
| | | Cd2–O41 | 2.416(16) | Zn2–Cl2 | 2.2149(15) | | |
| Nx–Cu–Ny | 84.7(2)–91.5(2); 177.0(2) | Nx–Cd–Ny | 87.3(2)–89.95(2); 177.1(2) | | | | |
| Nx–Cu–Cly | 84.31(2)–97.8(2); 169.1(2) | Nx–Cd–Cly | 82.4(2)–98.2(2); 171.4(3); 174.7(6) | Ex–Zn–Ey; Zn = Zn1, Zn2, E = N, Cl; (tetrahedral) | 102.34(18)–117.89(12) | Ex–Mn–Ey (octahedral) | 85.8(2)–93.4(2); 176.2(2)–179.1(2) |
| Cl1–Cu1–Cl2 | 172.73(7) | Cl1–Cd1–Cl2 | 167.30(5) | Ex–Zn3–Ey | 87.40(14)–91.93(15) | | |
| | | | | E = O, N (octahedral) | 177.69(15)–178.83(13) | | |
| #a: $-x+1/2, y-1/4, z+1/4$ #b: $x-1/4, y-1/4, -z+2$ | | #a: $-x+3/2, y+1/4, z-1/4$ #b: $x-1/4, y+1/4, -z+1/2$ | | #b: $1-x, -y, 2-z$; #c: $-1/2+x, 1/2-y, -1/2+z$; #e: $1/2+x, 1/2-y, -1/2+z$; | | #a: $-x+1/2, y, z-1/2$; #b: $x+1/2, -y+1$ | |

The observation of a zeolitic framework, natural for regular tetrahedral building blocks, was one of the desired targets of this investigation, even if its formation was not possible to predict. The structure is potentially porous, with 64.1% of solvent accessible volume for **1** and 61.6% for **2** (calculated by SOLV, PLATON),[36] provided that the solvent molecules are removed; averaged values for structures with and without the two-positionally disordered chloride atoms are given. The simulated surface areas[37] based on structural data are 1789 $m^2\ g^{-1}$ and 2132 $m^2\ g^{-1}$ for **1** and **2** respectively (the same averaging was used). The details on the experimental sorption study for **1** are given below.

**Structure of $[Zn_3Cl_2L(DMF)_4]\cdot 2DMF$, 3.** Two of the three zinc atoms in **3** have a tetrahedral $\{ZnCl_2N_2\}$ coordination environment and participate symmetrically in the formation of a binuclear $\{Zn_2(\mu\text{-tetrazolate})_2(\text{tetrazolate})_2Cl_2\}$ arrangement (Fig. 2b). In contrast, the third Zn atom has a *trans*-$\{ZnN_2O_4\}$ environment with two tetrazolate and four *N*,*N*-dimethylformamide ligands. Thus, less affinity to chloride anions is observed compared to the copper and cadmium compounds of **1** and **2**: despite the high concentration of the $ZnCl_2$ in the reaction medium a complete stripping of chloride coordination environment is observed for the Zn3 atom, while the retained chlorido ligands at Zn1 and Zn2 are bound terminally. The Zn–N and Zn–O bond lengths are fairly uniform, being in the range of 2.00–2.07 Å and 2.07–2.11 Å respectively, with the exception of the elongated Zn3–N7 bond (2.21 Å).

Overall the structure of **3** is a 3D coordination polymer with a complex connectivity. The binuclear $\{Zn_2(\mu\text{-tetrazolate})_2(\text{tetrazolate})_2Cl_2\}$ zinc cluster is connected to three $\mu_8$-$L^{4-}$ ligands and *vice versa*. All the tetrazolate groups of the latter are involved in metal coordination. Two of them bridge the two zinc atoms in a μ-κN2:κN3 'pyrazolato' fashion, while the other two coordinate them externally, in a tweezer-like way. The combination of the binuclear zinc clusters and the ligand is a dense 2D layer with a **fes** ($4\cdot8^2$) topology (Fig. 2d). The tetrazolate groups, which are 'tweezing' the binuclear cluster, are μ-κN1:κN3 'imidazolate' bridges and form coordination bonds also with the octahedral zinc ions (Fig. 2c), which stitch together the **fes** layers (Fig. 2e). The topology of the structure, thought as composed of the three connected nodes represented by the binuclear clusters and five connected nodes represented by the ligand, corresponds to an **fsc**-3,5-*Cmce*-2 net with a $\{4\cdot6^2\}\{4\cdot6^6\cdot8^3\}$ total point symbol as given by TOPOS.[60]

There are five known coordination polymers with this topology.[61] In all cases these are mixed-ligand [M(4,4′-bipy)L] (M = Zn, Mn, Co, Ni) compounds in which 4,4′-bipyridyl connects the 2D **fes** subtopologies constituted by the second ligand, typically a flexible dicarboxylate. Due to flexibility of the second ligand the structures do not serve as clear examples of pillaring design associated with the incorporation of rigid planar topologies.

In this regard **3** represents a unique example of a rigid structure with **fsc**-3,5-*Cmce*-2 topology, but its formation is not clearly rationalizable. Alternatively, the structure could be interpreted as composed of 1D parallel $\{Zn_2Cl_2(\text{tetrazole})_2\}\{Zn(\text{tetrazole})_2\}$ chains running along $[10\bar{1}]$ (a repeating part of the

 

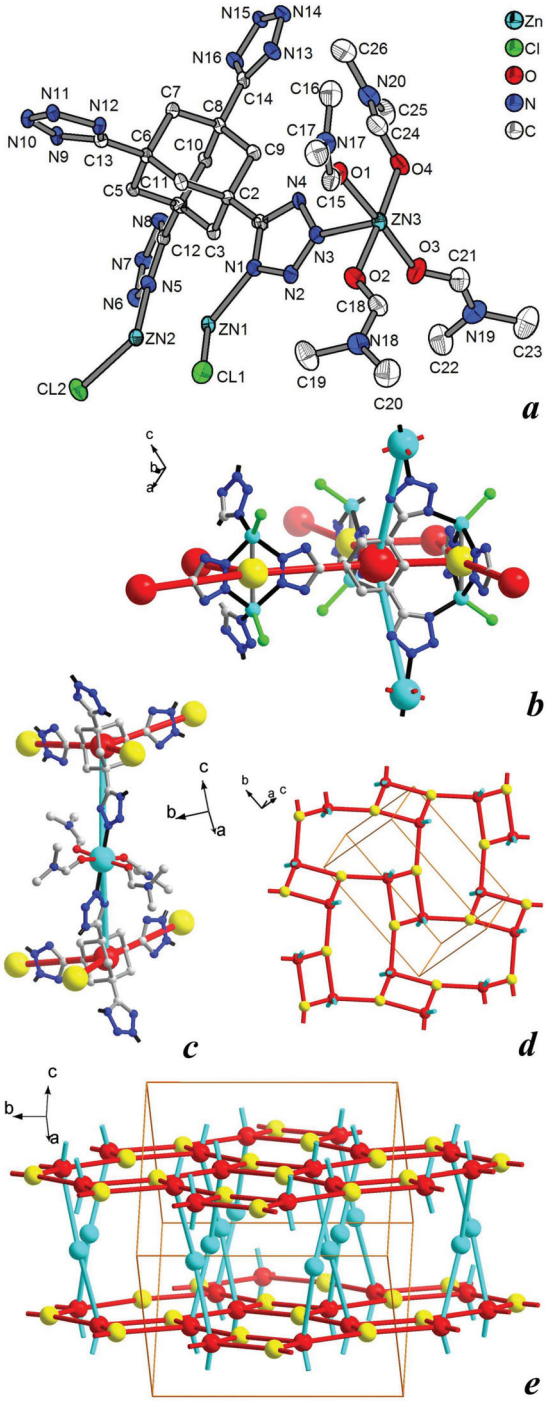


**Fig. 2** Structure of $[Zn_3Cl_2L(DMF)_4]\cdot 2DMF$, **3**. (a) ORTEP drawing of the asymmetric unit at the 50% probability level. (b) Topological environment of the ligand node (red) and the binuclear cluster node involving Zn1 and Zn2 (yellow). (c) Connection mode by the [Zn(tetrazolate)$_2$-(DMF)$_4$], the Zn3 atom is shown as a large blue sphere on other parts of the image. (d) A 2D layer with a **fes** topology, sustained by the binuclear clusters. (e) Topological representation of the structure, interpreted as stacked **fes** topologies.

chain is shown in Fig. 2b, right, marked by a blue zig-zag). The coordination-bonded chains are isolated from each other by the core of the adamantane ligand.

The space between the 2D sheets, or, alternatively, between the 1D chains are filled with four coordinated and two non-coordinated DMF molecules. The framework is porous with ~59% of solvent accessible voids (SOLV, PLATON)[36] and the simulated surface area is 2471 $m^2\ g^{-1}$.[37] According to the structural data, direct degassing at an elevated temperature ($T$ > 170 °C) is not a good option for generation of the porous structure due to probable collapse of the framework. Indeed, the coordination number of the 'pillaring' zinc atoms shrinks to two making possible rearrangement of coordination bonding network very probable. The availability of multiple donors at the tetrazolate group obviously facilitates such a rearrangement.

**Structure of $[Mn_2L(DMF)_2(MeOH)_4]\cdot DMF\cdot 2MeOH\cdot 2H_2O$, 4.** Compared to the previous compounds, **4** contains no chloride, *i.e.* complete chloride substitution from the coordination sphere during crystallization took place.

Two manganese atoms are bridged by three tetrazolate groups to form a binuclear three-blade paddle-wheel arrangement, typical for azole and azolate complexes, particularly for 1,2,4-triazole ones[1] (Fig. 4d). The arrangement is symmetric, with Mn–N bond lengths in the range of 2.23–2.27 Å, and Mn–N–N angles in the range of 121.6–130.4°. One tetrazole group of the ligand remains non-coordinated and disordered about an imaginary $C_3$ axis, corresponding to the triangular role of the ligand with three tetrazolates involved. The *fac*-{$MnN_3O_3$} arrangement is completed by DMF and MeOH solvent molecules (Fig. 3) and the binuclear clusters are combined by the effectively trigonal ligand to a honeycomb network (**hcb**, (6,3) hexagonal plane net).

The exact identity of the coordinated solvent molecules determined by the single-crystal diffraction study is questionable due to heavy disorder. The collected data clearly indicate that not all coordinated solvent molecules could be ascribed to DMF. It is unusual, as DMF is a more potent ligand compared to MeOH or water (at least according to relative 'donicities'[62]). Moreover, the assigned environment with three MeOH and three DMF molecules (Fig. 3a) introduces dissymmetry in the otherwise chemically equivalent metal centers. The asymmetry is possibly caused by the protruding non-coordinated tetrazole group, which blocks the necessary space. The short distance between two Mn metal centers ($d_{Mn1-Mn2}$ = 9.7 Å) also does not give sufficient space for localization of the two DMF molecules. Thus the proposed model is self-consistent, but it is only one of the most probable arrangements. Due to disorder some closely disposed pairs of solvent molecules could occupy the sites 'invertedly', with minor influence on the steric relations with other neighbours. The two *fac*-{$MnN_3O_3$} metal atoms were considered equivalent in the model describing the registered magnetism (see below).

The 2D honeycomb layers are stacked along the [010] direction (Fig. 3c). The packing is loose, only 30.9% (SOLV, PLATON)[36] of the space is filled by the solvent-free layers. Very close packing is impossible due to non-coordinated tetrazole groups protruding in the interlayer region. But even within this loose packing there is some steric concurrence between

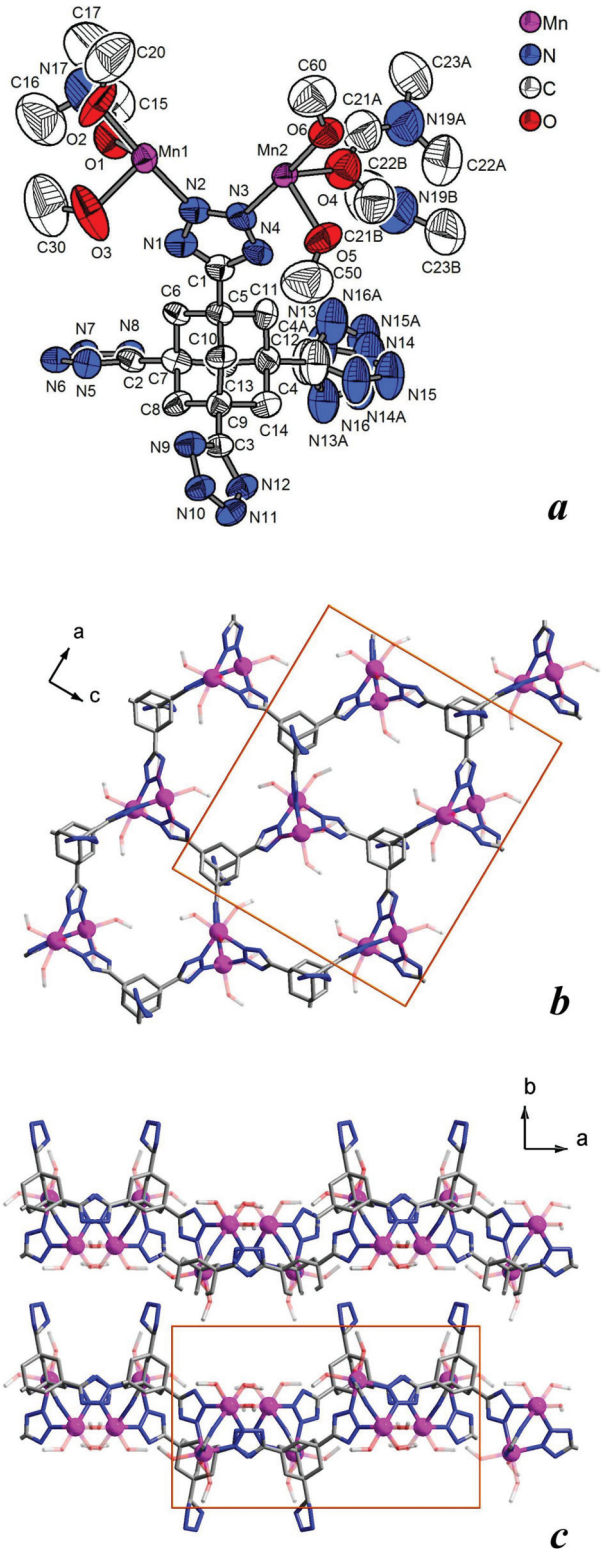


Fig. 3 Structure of $[Mn_2L(DMF)_2(MeOH)_4]\cdot DMF\cdot 2MeOH\cdot 2H_2O$, **4**. (a) ORTEP drawing of the asymmetric unit at 30% probability level. (b) A representative fragment of the 2D network sustained by $\{Mn_2(tetrazolate)_3(Solv)_6\}$ clusters. The disordered coordinated solvents are given partially and shown faded. (c) Perpendicular view of the 2D layer.

the coordinated solvent molecules, which conditions the coordination of MeOH molecules instead of DMF in some cases as described above. When 4 MeOH and 2 DMF are accounted as coordinated solvent molecules, the residual solvent accessible void volume is ~437 Å$^3$, which is roughly consistent with the ascribed composition of non-coordinated solvent molecules: 1 DMF (~127 Å$^3$), 2 MeOH (2 × ~67 Å$^3$) and $2H_2O$ (2 × ~40 Å$^3$) with a packing factor of 0.78 (see ESI‡ for explanation). The value does not contradict to TGA (Fig. S14‡); however, it is in moderate discrepancy with the elemental analysis data. Unlike the previous compounds, where the structural data are sufficient for precise identification of solvent content, the assignment of elemental composition for compound **4** is subject to a significant error primarily because it loses solvent molecules easily and as there is no clear criteria for drying the freshly prepared compound.

Regarding the imprecise elemental analysis, it is characteristic for all the reported compounds because of occlusion and cocrystallization with solvated metal salts, whose removal by washings is not efficient. As a note concerning elemental analysis, it is worth to add that high errors in nitrogen content determination could be observed in publications devoted to tetrazolate complexes,[30] and the conjectured reason is the presence of a ligand enriched phase either occluded or adherent to the surface of the material.

**Synthetic considerations and stability of the complexes.** The syntheses of the coordination polymers were performed by modifying a general approach based on heating of a solution of anhydrous metal chloride taken in approximately three-fold stoichiometric excess and $H_4L\cdot 3H_2O$ in DMF at 70 °C. The solubility of all compounds in the mother liquor is high, which explains the low yield of compounds **1–3** (~30%). **4** does not crystallize from DMF solution without the addition of MeOH, which decreases the solubility and assures a high yield (87%). Addition of methanol increases the yield in all cases, but the product's crystallinity was sufficient only in the case of **4**. The high observed solubilities in DMF indicate a high level of reversibility of the crystallization of tetrazolate coordination polymers and a concurrence between the chloride and the tetrazolate ligands.

The presence of water also has a significant effect on the crystallization process. The yield of **1** as well as its quality are slightly higher, when small scale experiments are carried out (a result of multiple observations), which seem to be the effect of trace amounts of water on the walls of the flask. The use of $CuCl_2\cdot 2H_2O$ instead of anhydrous chloride and a 4 : 1 v/v DMF–MeOH mixture affords blue crystals, which under prolonged heating eventually transforms, at least partially, to a product similar to the described $\{[Cu_4(\mu_4\text{-}Cl)(Ad(Tt)_4)_2]_2Cu\}\cdot 9DMF$ with a fluorite underlying net.[18] Thus the mixture of $M^{2+}$–$L_{tetrazolate}$–chloride could be viewed as a ternary coordinative system with possibly a number of co-existing compounds.

Chloride is a crucial additive: according to our preliminary experiments a completely different crystalline phase is formed, when the crystallization is performed starting from

 

$Cu(NO_3)_2{\cdot}3H_2O$ in water solution (blue blocks, monoclinic, $C2/c$, $a$ = 43.075, $b$ = 12.993, $c$ = 20.381, $\beta$ = 109.25).

Despite the possible advantageous effect of water as a minor component of the solvent mixture, compounds **1–4** are not stable under air due to the presence of moisture. A significant change of PXRD patterns took place within tenth of minutes or hours (Fig. S20, S21, S23 and S24‡). While **4** is generally unstable and the primary factor of crystallinity loss is seemingly efflorescence, in other cases a slow conversion to another phase is observed rather than an immediate amorphisation. It could be associated with partial hydrolysis of the M–Cl bonds, especially in the case of the zinc complex **3**. The crystals of the copper complex **1** slowly adopt a bluish tint supporting the involvement of water in the coordination sphere (Fig. S20‡). Most probably the terminal chloride, which is disordered in the crystal structure, is exchanged in the first place. The relatively stable transient phases suggest a rich coordination chemistry of mixed hydroxy-(oxo-)/chlorido-/tetrazolato complexes and controlled solvolysis as a method of synthesis for some of them.

**1–4 as representatives of M(II)/tetrazolato/halido systems.** According to the search in CSD[31] there are 194 structures of transition metal complexes with tetrazolato/halido ligands, with the majority of them containing chlorido ligands. This set constitutes a significant part of all known 1352 tetrazolate complexes and demonstrates high probability of ligand synergy. The multitude of binding modes exhibited by tetrazolate prevents simple classification and this is why, according to our knowledge, there is yet no review scrutinizing the structural trends for these compounds. Their importance for the formation of notable tetrazolate-based frameworks[8,9] is recognized and some examples of tetrazolato/chlorido coordination bonded clusters are non-systematically reviewed.[7,32] The special role of chloride in the formation of mixed-ligand complexes of cadmium and 5-(pyridyl)tetrazolate was also scrutinized.[33]

The present contribution could be viewed as an attempt to investigate the possibilities provided by the synergy between a small 'tetrahedral' tetrazolate and chloride ligands. Short chloride bridges allow the completion of the coordination environment together with charge control (unlike the case of solvent coordination). The principle of inclusion of a short bridge in a prototypal motif based on μ-azole(ato)-$\kappa^2$-N1,N2 bridging ligands is shown in Fig. 4a (62 out of 194 mixed-ligand tetrazolato/halido complexes of transition metals[31] contain this motif with Fn = μ-halido and tetrazolato ligands involved either as $\kappa^2$-N1,N2 or less frequently as $\kappa^2$-N2,N3 bridges). This prototypal motif could be a part of a chain of indefinite length or, formally, a part of a very important cyclic motif, exemplified by $\{M_4Cl(tetrazolate)_8\}$.[16–18,41] The halido- or oxo-/oxido- bridges mediate the connectivity, while the additional donor atoms of the tetrazolate ligand allow additional binding modes, which explains the high geometric variability of the mixed ligand coordination bonded clusters. The obtained compounds are based on variations of this generalized motif (Fn = -, Cl, tetrazolato), depicted in Fig. 4b–d.

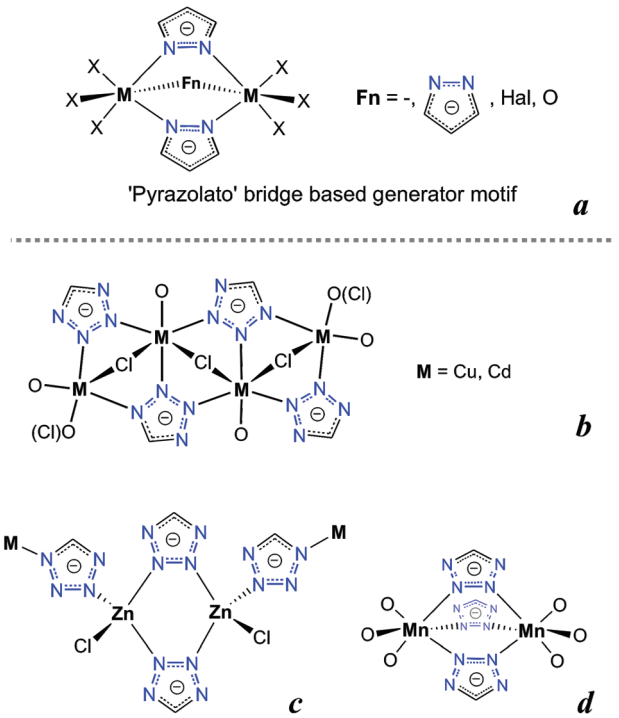


**Fig. 4** The generator motif by μ-azolate-$\kappa^2$N1,N2 type ligands (a), and its actualizations for the reported complexes of $H_4L$: direct as in the case of **4** (d), or with involvement of additional bonding opportunities provided by the tetrazolate function as in **1**, **2** (b), or **3** (c).

The tetranuclear pattern in Fig. 4b, found in compounds **1** and **2** is not elementary, but could be thought as an extension of a trinuclear minimal sequence. An infinite chain of this type is found in $[Mn_2(BDT)_8Cl_2(DMF)_2]$ ($H_2BDT$ = 1,4-di(tetrazol-5-yl)benzene).[8] The coordination-bonded pattern observed in **3** (Fig. 4c) has no precedents; however, loose analogs could be found in five compounds of copper and cadmium, but in all cases a μ-Cl bridge connects the two metal atoms. The three-blade paddlewheel cluster (**4**, Fig. 4d) realized without the involvement of non-azolate bridging groups is not tetrazolate specific, but often registered in other azolate and azole complexes, especially in 1,2,4-triazole[1] ones. In addition to the case of compound **4**, it is realized also in $[Mn_4(BDT)_3(NO_3)_2(DEF)_6]$ in a binuclear version and in $[Mn_4(BDT)_3(NO_3)_2((DEF)_6]$ in an extended trinuclear version.[8]

The variability of the mixed tetrazolato/chlorido clusters allow to view them as compliant joints allowing a structural 'imprinting'[20] by the high-symmetry ligand *i.e.* the structure-defining role of the rigid ligand, when the coordination-bonded cluster is not predefined, but could adopt various geometries, or in other words is structurally malleable. Example of such imprinting associated with non-tetrazolate 'tetragonal' ligands could be found for example in the diamondoid structure of $[Ag_4(1,3,5,7\text{-tetrakis}(4,4'\text{-sulfophenyl})adamantane)(H_2O)_2]{\cdot}1.3H_2O$,[12] where the high-density of the donor sites allowed the complex coordination-bonded cluster to follow the simplest assembly approach dictated by the highly symmetric ligand.

In the current study such 'imprinting' indeed took place for the zeolitic structures of **1** and **2**, but was not achieved for the other two cases, which is interpreted as partial or complete failure to secure the incorporation of chloride anions. Hence, the more rigid spatial requirement of the tetrazolate-only coordination environment disallowed the assembly governed by the ligand's symmetry. In general there is also a clear tendency towards expression of the ligand in a triangular mode, *i.e.* the structures of **3** and **4** express lamination and a distinct 'polar' direction perpendicular to the layers.

We consider the experimentation with tetrahedral tetrazolate ligands in the presence of chlorides as an empirical tool for searching promising structural motifs. The latter could be prototypal for more stable azolate analogs considering tetrazolate as a mimic function.[18] Among the reported series of compounds the most interesting prototypal structure organization, which is chloride-free, could be found in **4**. The layers supported by binuclear clusters could be stacked by the use of the hexafunctionalized 1,1′-biadamantane ligand to form a bilayer or a 3D framework structure. Other methods of synthesis, particularly hydrothermal synthesis, might provide unusual structural organization, also based on infinite coordination-bonded clusters akin to or denser than those found in **3**.

### Sorption studies of degassed $[Cu_4Cl_4L(DMF)_5]\cdot DMF$, 1

Compounds of copper and cadmium, **1** and **2** with a robust zeolitic framework structure have good prerequisites for permanent porosity after the removal of solvent molecules. Direct degassing at elevated temperatures was anticipated to be non-productive as slow decomposition of the ligand starts slightly over 200 °C, while the copper compound is reductively unstable at temperatures over 80 °C due to the presence of DMF. A solvent exchange strategy was used to reduce the temperature of degassing and to challenge the activation of structurally less stable compounds of zinc **3** with an expectedly labile framework and manganese **4** with a layered non-framework structure. A uniform procedure of activation, involving soaking in methanol for at least 5 days with subsequent mild degassing at 30 °C–120 °C was applied for all compounds (additional details are given in the ESI‡). Compounds **2–4** did not demonstrate measurable adsorption of nitrogen, but non-negligible hydrogen sorption was registered (77 K, for 1 g at STP: 7.5 $cm^3$ after degassing at 120 °C for **2**, 23.3 $cm^3$ at 70 °C for **3** and 16.9 $cm^3$ at 70 °C for **4**; see Table S5‡). Obviously only partial solvent exchange was reached in these cases and the process was not efficient. The sorption of hydrogen by the zinc compound **3** decreases with increase of temperature supporting the anticipated low stability of the framework (see ESI‡ for additional discussion on negative results).

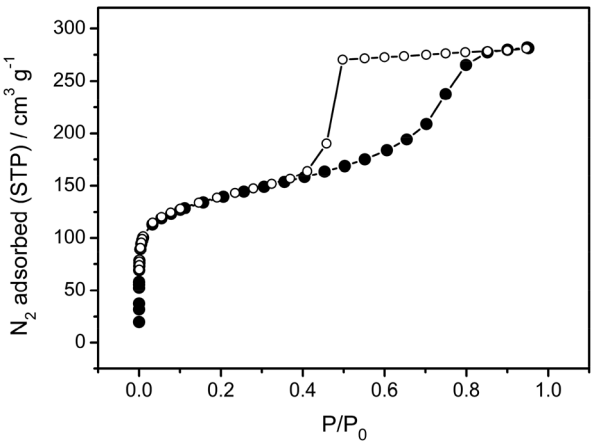


Fig. 5 $N_2$ sorption isotherm at 77 K for the activated **1**.

In contrast, the solvent exchange process in **1** proved to be quite efficient. Optimized exchange experiments showed that ~20 days soaking in methanol at RT with periodic refreshing of the supernatant liquid or 5 days soaking at 70 °C are roughly equivalent in efficiency yielding the removal of almost all of the DMF residing in the pores, as evidenced by IR spectroscopy (Fig. S16‡). Longer soaking times did not improve the depth of the exchange significantly, but rather caused deterioration of the material and discharge of some amount of fine precipitate.

The adsorption isotherm (Fig. 5) for $N_2$ at 77 K is of type II with a $S_{BET}$ = 505.5 $m^2\ g^{-1}$ ($P/P_0$ = 0.03–0.11; $S_{Langmuir}$ = 594 $m^2\ g^{-1}$ for the same data points) compared to 1789 $m^2\ g^{-1}$ of the simulated Connoly surface based on the structural data (Table 2).[37] The total pore volume is 0.435 $cm^3\ g^{-1}$ (or 0.469 $cm^3\ cm^{-3}$ at $\rho$ = 0.927 g $cm^{-3}$ compared to 0.641 $cm^3\ cm^{-3}$ by the structural data) at $P/P_0$ = 0.95. The desorption isotherm is of type IV with a lower closing point at $P/P_0 \sim 0.4$, corresponding to a mesoporous material (the typical closure point is $P/P_0$ = 0.42[38]). Two independently processed samples demonstrated the same unexpected characteristics (Fig. S27‡). The hysteresis loop shape is known as H2 type hysteresis and occasionally found in silica-

Table 2 Summary of topology, symmetry, porosity and magnetism related parameters for **1–4**

| Compound | Topology; symmetry | Surface area calculated (experimental)/$m^2\ g^{-1}$ | Porosity calculated (experimental)/$cm^3\ cm^{-3}$ | $J$, coupling parameter/$cm^{-1}$ |
|---|---|---|---|---|
| $[Cu_4Cl_4L(DMF)_5]\cdot DMF$, **1** | $\{4\cdot6^2\}\{4\cdot6^6\cdot8^3\}$ **gis**; *Fddd* | 1789 (505.5) | 0.641 (0.469) | −9.60(1), −17.2(2), −2.28(10) |
| $[Cd_4Cl_4L(DMF)_7]\cdot DMF$, **2** | $\{4\cdot6^2\}\{4\cdot6^6\cdot8^3\}$ **gis**; *Fddd* | 2132 | 0.616 | — |
| $[Zn_3Cl_2L(DMF)_4]\cdot 2DMF$, **3** | $\{4\cdot6^2\}\{4\cdot6^6\cdot8^3\}$, **fsc**-3,5-*Cmce*-2; $P2_1/n$ | 2471 | 0.59 | — |
| $[Mn_2L(DMF)_2(MeOH)_4]\cdot DMF\cdot 2MeOH\cdot 2H_2O$, **4** | $\{6^3\}$, **hbc**; $Pca2_1$ | — | 69.1 | −0.76(2) |

 

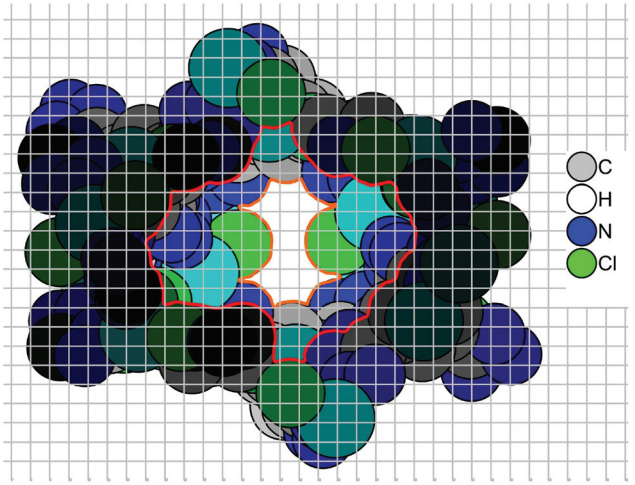


**Fig. 6** Pore cross-section in **1** with gradiental dimming (close atoms are darker) and a grid overlay with a 1 Å step. The red line approximately limits the internal cavity's cross-section (~7 × 13 Å), the orange line limits the pore entrance (<3 × 5 Å).

gels. The H2 type is associated with the presence of narrow 'neck-pores' and wide 'body-pores', though this explanation is regarded as simplified.[38]

According to the crystal structure with the solvent molecules removed, the pores in **1** should indeed have a narrow entrance 'padded' by chloride (Cl2) ions and having a size less than 3 × 5 Å, just sufficient for the entrance of $N_2$ gas molecules, and more spacious inner cavities (Fig. 6). But there is, of course, no mesoporosity, as it is witnessed by the determined crystal structure. NLDFT calculations using a 'cylinder pores in silica' model (as implemented in the ASiQwin 2.0 software, either using adsorption branch or equilibrium approaches) points out that there are two dominant pore radii, at ~5 Å, which roughly corresponds to the pores observed in the structure and a range of mesopores with the most probable radii at 26–37 Å depending on the model (Fig. S32‡). If the mesoporosity, which should not be present according to the structural data, had been attributed to textural effects, *i.e.* additional uptake attainable to the rough surface of the particles and secondary structures formed by them, it would give only a relatively small increment of surface area, but according to the calculations it would add ~1/4 of the observed microporous surface area, which is an unprobably large value. Moreover, the H2 type hysteresis is not typical for simple mesoporous capillaries with a constant width, for which the adsorption and desorption branches should be more similar, *e.g.*, H1 type or H3, H4 types for non-cylindrical pores. The low slope of the desorption branch near the high point of closure reflects hindered evaporation of the adsorbate, *i.e.* a 'gate' effect is observed.[39] It is an open question, whether the gate effect could be ascribed to the narrow pore entrances, but in any case it would be next to impossible to explain the obvious mesoporous nature of the effect. We believe that the observed effect is not a static, but rather a dynamic one. The specific hysteresis pertains to structural transformation of the framework and a possible 'gate' effect associated with it. This viewpoint is illustrated more quantitatively by the NLDFT calculations (Fig. S32‡): the formal pore diameters in the mesoporous region calculated from the adsorption branch have a very broad spread ($d$ = ~38 ± 13 Å) corresponding to sequential 'inflation' of the structure, while the diameter range calculated from the desorption branch is much narrower ($d$ = ~26 ± 4 Å) explained by a more uniform 'deflation' process. The hypothesis of the framework's transformation also explains the discrepancy between the relatively consistent total pore volume at $P/P_0$ = 0.95 but small surface area of the sample.

Due to the observed effect **1** is a prominent candidate for further investigations, aiming at framework flexibility based on coordination-bonded cluster transformations. Tetrazolates, with an especially high density of donor atoms are especially promising objects for such search.

Numerous UMSs in activated **1** are a nice prerequisite for effective hydrogen sorption. In this regard the material is not very remarkable though, demonstrating 0.72–0.79 wt% $H_2$ adsorption at 77 K and 1 bar depending on the sample (Fig. 7). The zero-coverage isosteric heat of adsorption at 77–87 K was calculated to be −7.2 kJ $mol^{-1}$ using the Clausius–Clapeyron equation and the adsorption data collected at liquid nitrogen and liquid argon temperatures (Fig. S31‡). This value is in the range of 6.8–9.5 kJ $mol^{-1}$ values[40] observed for the best copper complexes,[41] with the highest value belonging also to a tetrazolate complex $HCu[(Cu_4Cl)_3(BTT)_8]$. The value obtained for the prototypal HKUST-1 using an independent spectroscopic approach is ~10.1(7) kJ $mol^{-1}$ at 80–150 K,[42] though only 5.0 kJ $mol^{-1}$ was confirmed experimentally.[35] The adsorption of hydrogen at 293 K and 1 bar amounts to a meager ~0.06 wt% (Fig. S29‡), but it significantly exceed the interpolated value for MOF-5[43] or HKUST-1 (0.1 wt% at 20 bar;[35] the dependence is practically linear in the 1–20 bar pressure) and also much more than the measured ~0.01 wt% (298 K, 1 bar) for single walled nanotubes (SWNT)[44] or for active carbons (the interpolated value is $8 \times 10^{-3}$–$1 \times 10^{-2}$ wt% at 298 K).[45] Interestingly, the affinity towards hydrogen is strong and the desorption is

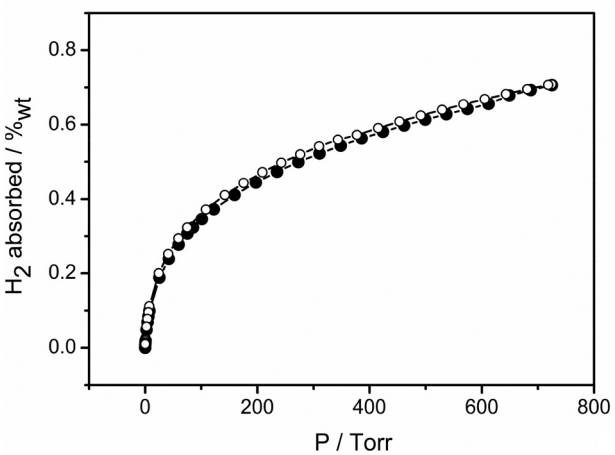


**Fig. 7** $H_2$ sorption isotherm at 77 K for the activated **1**.

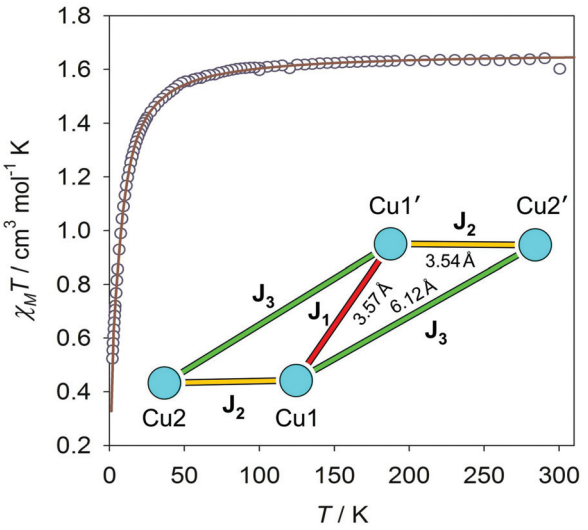


Fig. 8 Temperature dependence of the $\chi_M T$ product for **1** and the fitting function for the tetranuclear model. The coupling scheme is given on the expansion.

almost absent on the time-scale of minutes, however it might be only a kinetic effect.

### Magnetic measurements on 1 and 4

The temperature dependence of the molar magnetic susceptibility and temperature product, $\chi_M T$ *vs.* $T$, for **1** in the range of 1.9–300 K is depicted in Fig. 8.

The $\chi_M T$ value at room temperature is 1.61 cm$^3$ mol$^{-1}$ K, a value expected for four magnetically isolated Cu(II) ions [$\chi_M T = 4(N\beta^2 g^2/3kT)S(S + 1)$ = 1.65 cm$^3$ mol$^{-1}$ K with $g_{Cu}$ = 2.1 and $S_{Cu}$ = 1/2][46] and it decreases continuously from room temperature to 1.9 K. This decrease is very slow at high temperatures, but below 100 K it becomes more pronounced. These features are indicative of a dominant weak antiferromagnetic interaction in **1**. As the clusters are well separated by adamantane moiety inserts, they could be regarded as magnetically isolated (closest intercluster Cu–Cu distance is 8.00 Å). The elongated chain-like {$Cu_4$} cluster[46] is regarded as constituted of halves related by symmetry, which is a minor simplification taking into account the disordered terminal chloride anions. Any of the copper atom pairs except the two terminals are joined by tetrazolates acting as μ-κN1:κN2 and μ-κN1:κN2 'pyrazolato' and/or $\mu_2$-'imidazolato'-κN1:κN3 type bridges, characterized by $J_1$ and $J_2$ coupling constants for 'pyrazolato' and $J_3$ for 'imidazolato' bridges (Fig. 8 and 4b).

The zero-field spin Hamiltonian is given by the equation:

$$\hat{H}_1 = -J_1(\hat{S}_1\hat{S}_{1'}) - J_2(\hat{S}_1\hat{S}_2 + \hat{S}_{1'}\hat{S}_{2'}) - J_3(\hat{S}_1\hat{S}_{2'} + \hat{S}_{1'}\hat{S}_2)$$

A similar coupling scheme is found in some alkoxo-bridged Cu(II) halido complexes with double defective cubane structures for which the temperature dependence of the magnetic susceptibility data has been reported and analyzed previously.[47,48] Least-squares fitting of the data for compound **2** gave the next values for the parameters: $g$ = 2.10(1), $J_1$ = −8.5(1), $J_2$ = −4.80(2), $J_3$ = −1.15(10) cm$^{-1}$ and $R = 2.30 \times 10^{-5}$ (where $R$ is the agreement factor defined as $\sum_i[(\chi_M T)_i^{exp} - (\chi_M T)_i^{calc}]^2/\sum_i[(\chi_M T)_i^{exp}]^2$). The fitting matches very well with the experimental data in the whole temperature range (Fig. 8). The small value of $J_3$ is in accordance with the expectations due to the large Cu(II)–Cu(II) distance sustained by the 'imidazolato' bridge. The result of the fitting points at two salient features: the observed weak magnetic coupling mediated by the tetrazolate bridge is in contrast with the moderate-strong antiferromagnetic coupling observed for pyrazolate- and triazolate-bridged copper(II) complexes,[49,50] and, secondly, the $J_1$ is significantly larger than $J_2$, even though both parameters correspond to the same type of μ-κN1:κN2 'pyrazolato' bridges. A detailed account of the main structural features governing the magnetic interaction of copper(II) complexes bridged by 'pyrazolato' and/or 'imidazolato' linkers can explain these facts. The affecting parameters are: (i) the nature of the azolate ligand (given by the number of N-atoms), (ii) the configuration of the coordination environment, *i.e.* square-pyramidal *vs.* trigonal-bipyramidal geometry ($\tau$ = 0.06),[34] the Cu–N–N–Cu torsion angle value and (iii) the degree of the asymmetry of the bridge.[51] The increase in the number of electronegative N-atoms in the azolate ligands decreases the energy of orbitals, including the ones associated with the formation of the coordination compounds. This is equivalent to decrease of the antiferromagnetic coupling between the copper(II) ions, bridged by such azolate ligands. The trigonal distortion also has an important effect. The $d_{x^2-y^2}$ orbital of copper(II) ions in pure tetragonal-pyramidal or octahedral geometry is singly occupied (either basal or equatorial). However, the trigonal distortion withdraws spin density from the $d_{x^2-y^2}$ orbital into the $d_{z^2}$ orbital (axial) which has usually longer bond distances because of the Jahn–Teller distortion and those larger distances and the removal of spin density from the equatorial sites lead to weaker magnetic coupling. The stronger coupling observed for $J_1$ occurs because $J_2$ is associated with highly asymmetric bridging, in which case the interactions are weaker.[52] Indeed, $J_2$ is associated with bridging, which involves Cu–N distances of 2.033(5) Å and 2.466(5) Å and Cu–N–N angles of 126.5(4)° and 110.65(4)°, whereas $J_1$ is associated with rather symmetric bridges with 2.033(5) Å and 2.002(5) Å bonding distances; and 123.7(4)° and 125.7(4)° bonding angles. Moreover, the $J_1$ exchange pathway is associated with tetrazolates coordinated in the equatorial positions, whereas for $J_2$ one of the tetrazolates is coordinated to the axial position. All the listed aspects accounts for the weaker coupling through $J_2$.[53–55]

The temperature dependence of the $\chi_M T$ product for compound **4** is shown in Fig. 9. At room temperature $\chi_M T$ is 8.85 cm$^3$ mol$^{-1}$ K, a value which is close to that expected for two uncoupled Mn(II) ions [$\chi_M T = 2(N^2\beta^2 g_{Mn}{}^2/3kT)S_{Mn}(S_{Mn} + 1)$ = 8.84 cm$^3$ mol$^{-1}$ K with $g_{Mn}$ = 2.01, $S_{Mn}$ = 5/2].[46] On lowering the temperature it remains almost constant till 100 K and below this temperature there is a sharp decrease resulting in a drop of $\chi_M T$ to 3.37 cm$^3$ mol$^{-1}$ K at 2 K. These features are

 

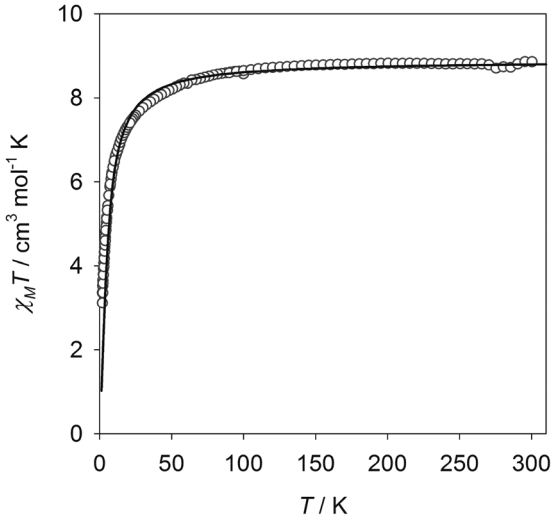


Fig. 9 Temperature dependence of the $\chi_M T$ product and the fitting function for **4**.

indicative of a weak antiferromagnetic interaction between the Mn(II) dimers in **4**.

The manganese dimers are isolated by the adamantane inserts and could be regarded as isolated (the closest intercluster Mn–Mn distance is 9.21 Å). The magnetic interaction within the dinuclear manganese clusters sustained by three 'pyrazolato' type bridges is described by the equation given below,[46] which is derived from the isotropic spin Hamiltonian for two communicating nuclei:

$$\hat{H}_2 = -J(\hat{S}_1\hat{S}_2)$$

$$\chi = \frac{2Ng^2\beta^2}{kT}\frac{e^x + 5e^{3x} + 14e^{6x} + 30e^{10x} + 55e^{15x}}{1 + 3e^x + 5e^{3x} + 7e^{6x} + 9e^{10x} + 11e^{15x}}$$

with $x = J/kT$. The lest squares fitting gives the next values for the parameters: $g$ = 2.01(1), $J$ = −0.76(2) cm$^{-1}$ and $R$ = 1.20 × 10$^{-4}$ (where $R$ is the agreement factor defined as $\sum_i[(\chi_M T)_i^{exp} - (\chi_M T)_i^{calc}]^2/\sum_i[(\chi_M T)_i^{exp}]^2$). Tetrazolate bridges mediate very weak magnetic coupling between Mn(II) ions and similar values of $J$ have been reported for other Mn(II) complexes containing this kind of bridges.[56]

## Conclusions

The potential of a 'tetrahedral' tetrazolate ligands for synthesis of framework coordination bonded polymers was demonstrated along with the synergistic role of the halido bridges, which allows higher versatility and expandability of the coordination bonded cluster. Because of such synergy a zeolitic structure is realized in the copper and cadmium complexes; however, only the adamantane building block provides prerequisites for such behaviour. The effect, dubbed 'ligand imprinting', could be of general interest in the case of other mixed azolate/halido polymers and in this context the tetrazolate complexes serve as prototypes, which could emulate any other azolate binding mode.

Inclusion of the halido bridges, as it was shown in the copper complex of **1** allows the synthesis of a completely different structure compared with the known fluorite-type analog, albeit with potentially higher surface area. The yet not clearly understood specific sorption properties are seemingly associated with framework flexibility. The possibility of non-typical flexibility based not only on the change of the coordination bonded cluster's geometry, but also on partial rearrangement of the coordination bonding is especially feasible for the multidentate tetrazolate ligands and the observed effect is rather promising in this regard.

## Experimental

### Chemicals

Anhydrous $CdCl_2$, $CuCl_2$, $ZnCl_2$, $MnCl_2$, and $NaN_3$ salts (99%+) were commercial reagents and used without subsequent purification. *N*,*N*-Dimethylformamide (DMF) used for the synthesis of $H_4L$ was freshly distilled under reduced pressure after drying over $CaH_2$. Dimethyl sulfoxide (DMSO), DMF, and methanol (MeOH) for crystallization of coordination polymers (VWR, ACS) or for solvent exchange (Aldrich, spectroscopic grade) were used as delivered.

### X-ray structure determination

Selected monocrystals of suitable optical quality coated in perfluorinated oil were mounted on a glass fiber, transferred to diffractometer and measured at low temperatures under protective dinitrogen gas stream (crystal data, and details concerning data collection and refinement are given in Table 3). The data reduction was performed by SAINT and multi-scan adsorption corrections were implemented by SADABS for structures of **1** and **2**.[57] For structures of **3** and **4** an alternative data collection and reduction software were also used.[58] Lattice parameters, initially determined from more than 100 reflections, were later refined against all data.

Space group assignment was done using XPREP; the structures were solved by direct methods (SIR-92 or SHELXS-97) and refined by full-matrix least squares on $F^2$ method using SHELXL-97.[57,59] Non-hydrogen atoms were refined anisotropically, except a few special cases of disordered solvent molecules, which were refined in isotropic approximation.

The solvent molecules were modelled using bond length restraints and similarity-restraints of thermal displacement parameters.

The hydrogen atoms were placed on idealized positions and refined using a riding model with $U_{iso}(H) = kU_{eq}(C_{parent})$ ($k$ = 1.2 for the formyl group of DMF and methylene groups of the adamantane moieties and $k$ = 1.5 for methyl groups of DMF molecules). The hydrogen atoms of the disordered *N*,*N*-dimethylformamide molecule residing in the pores were not refined in the case of **2**, while in the case of **1** the whole molecule was excluded from the refinement using the SQUEEZE

**Table 3** Crystal data and structure refinement for $[Cu_4Cl_4L(DMF)_5]\cdot DMF$, **1**; $[Cd_4Cl_4L(DMF)_7]\cdot DMF$, **2**; $[Zn_3Cl_2L(DMF)_4]\cdot 2DMF$, **3**; $[Mn_2L(DMF)_2(MeOH)_4]\cdot DMF\cdot 2MeOH\cdot 2H_2O$, **4**[a]

| | 1 | 2 | 3 | 4 |
|---|---|---|---|---|
| Empirical formula | $C_{32}H_{54}Cl_4Cu_4N_{22}O_6$[b] | $C_{38}H_{68}Cd_4Cl_4N_{24}O_8$ | $C_{32}H_{54}Cl_2N_{22}O_6Zn_3$ | $C_{29}H_{61}Mn_2N_{19}O_{11}$[b,c] |
| Diffractometer | Bruker Apex II CCD | Bruker Apex II CCD | Bruker KappaCCD | Kappa CCD |
| $M_r$/g mol$^{-1}$ | 1238.93[b] | 1580.56 | 1109.99 | 961.85[c] |
| $T$/K | 113(2) | 113(2) | 123(2) | 173 |
| Wavelength/Å | 0.71073 | 0.71073 | 0.71073 | 0.71073 |
| Crystal system | Orthorhombic | Orthorhombic | Monoclinic | Orthorhombic |
| Space group | *Fddd* (no. 70) | *Fddd* (no. 70) | $P2_1/n$ | $Pca2_1$[d] |
| $a$/Å | 19.6939(4) | 20.8726(7) | 15.7345(5) | 21.439(4) |
| $b$/Å | 27.4554(4) | 27.5137(9) | 20.5801(4) | 12.674(3) |
| $c$/Å | 41.4894(9) | 43.5530(13) | 15.7442(4) | 18.917(4) |
| $\beta$/° | 90 | 90 | 112.1180(10) | 90 |
| $V$/Å$^3$ | 22 433.5(7) | 25 011.7(14) | 4723.1(2) | 5140.0(18) |
| $Z$ | 16 | 16 | 4 | 4 |
| Calc. density/g cm$^{-3}$ | 1.467 | 1.679 | 1.56102(7) | 1.243 |
| $\mu$/mm$^{-1}$ | 1.745 | 1.576 | 1.691 | 0.556 |
| $F$(000) | 10 112 | 12 608 | 2288 | 2024 |
| Crystal size/mm$^3$ | 0.15 × 0.1 × 0.1 | 0.17 × 0.13 × 0.13 | 0.10 × 0.08 × 0.04 | 0.19 × 0.16 × 0.03 |
| $\theta$ range/° | 5.13 to 23.73 | 4.08 to 27.10 | 3.27 to 27.52 | 5.10 to 25.32 |
| Index ranges/*hkl* | [−22;22], [−29;31], [−46;46] | [−27;20], [−35;30], [−57;57] | [−17;20], [−26;26], [−20;17] | [−25;25], [−15;15], [−22;22] |
| Reflections collected ($R_{int}$) | 57 043 (0.045) | 33 321 (0.0630) | 31 850 (0.0426) | 29 031 (0.0760) |
| Independent reflections | 4208 | 7429 | 10 695 | 9208 |
| Completeness/% to $\theta$/° | 98.6 to 23.73 | 99.6 to 27.10 | 98.3 to 27.52 | 98.8 to 25.32 |
| Absorption correction | Multi-scan | Multi-scan | None | Analytical |
| Max. and min. transmission | 0.8449 and 0.7798 | 0.8213 and 0.7754 | — | 0.9018 and 0.9835 |
| Data/restraints/parameters | 4217/160/346 | 6877/231/435 | 10 695/0/599 | 9208/317/533 |
| Goodness-of-fit on $F^2$ | 1.066 | 1.033 | 1.036 | 0.944 |
| $R_1$, w$R_2$ [$I > 2\sigma(I)$] | 0.0681, 0.1931 | 0.0521, 0.1359 | 0.0445, 0.1071 | 0.0654, 0.1693 |
| $R_1$, w$R_2$ (all data) | 0.0747, 0.1989 | 0.0750, 0.1528 | 0.0578, 0.1156 | 0.0884, 0.1813 |
| Largest diff. peak and hole, e Å$^{-3}$ | 1.882 and −1.144 | 2.002 and −0.951 | 0.839 and −0.755 | 0.379 and −0.348 |

[a] Full-matrix least-squares refinement on $F^2$. $R_1 = \sum||F_o| - |F_c||/\sum|F_o|$; w$R_2 = \{\sum[w(F_o^2 - F_c^2)]^2/\sum[w(F_o^2)^2]\}^{1/2}$ where $w^{-1} = [\sigma^2(F_o^2) + (aP)^2 + bP]$, $P = [2F_c^2 + \mathrm{Max}(F_o^2, 0)]/3$, $a$ and $b$ are refined parameters; GooF $= \{\sum[w(F_o^2 - F_c^2)^2]/(n - p)\}^{1/2}$. [b] SQUEEZE (PLATON) treatment is applied. The molecular weight is given with the solvent molecules excluded from the refinement. [c] Partial solvent molecule refinement. [d] Absolute structure parameter is 0.32(3).

(PLATON) procedure[36] due to complexity of the disorder. The latter procedure was also applied to **4**, as complete solvent molecule modelling was not possible.

The selected crystals of **3** and **4** were twins. In the pseudo-merohedral twin **3** the twin domains are related by a plane of symmetry with {−1, 0, 1} index (the SHELXL twin law matrix is 0 0 1 0 1 0 1 0 0). The weights of the twin domains are approx. 0.44/0.56. The inversion-twin **4** has a 0.68/0.32 component ratio.

The relatively high *R*-indices for the structure of **4** are explained by structural instability towards facile solvent loss by the thin platelet crystals. The correctness of structural determination of **1** is reinforced by its near isostructurality to **2**. Additional details concerning the refinement of structures **1** and **2** are given in the ESI.‡

## Analytics

Single crystal X-ray diffraction experiments were performed using a Bruker APEX II QUAZAR system equipped with a multilayer monochromator and a microfocused IMS molybdenum Kα source ($\lambda$ = 0.71073 Å). The PXRD measurements were performed on a finely ground sample equally distributed on a low background silicon sample holder using a Bruker AXS D2 PHASER instrument equipped with a Lynxeye 1D detector and using Ni-filtered copper Kα radiation (30 kV, 10 mA generator parameters; beam restricted by a 0.6 mm divergence slit and a 1° Soller collimator) at 0.02° measurement step width. The simulated PXRD patterns were generated using Mercury 2.3 program with 0.02° step and FWHM ($2\theta$) = 0.1° further scaled by an adapting exponential function aiming better correspondence to the experimental data. $^1$H and $^{13}$C spectra were recorded using Bruker Avance DRX-200 and Bruker Avance DRX-500 instruments respectively. FT-IR spectra were recorded using a Bruker Tensor 37 system equipped with an ATR unit (Platinum ATR-QL, Diamond) in the 4000–550 cm$^{-1}$ region with 2 cm$^{-1}$ resolution. Sorption measurements were performed using the Quantachrome iQ and Micromeretics ASAP 2020 automatic gas sorption analyzers. The thermogravimetric (TG-DTA) analyses were performed using a Netzsch STA 449 C Jupiter instrument coupled with a Pfeiffer Thermostar GSD 300 mass spectrometer at 5–10 °C min$^{-1}$ heating rate under inert gas flow using corundum sample holders. Alternatively, the TG data were collected using a Netzsch 209 F3 Tarsus instrument in a protecting flow of nitrogen (10 ml min$^{-1}$) at

 

5 °C $min^{-1}$ heating rate. Magnetic susceptibility measurements on polycrystalline samples were carried out in the temperature range 1.9–300 K by means of a Quantum Design SQUID magnetometer operating at 10 000 Oe. Diamagnetic corrections of the constituent atoms were estimated from Pascal's constants. Experimental susceptibilities were also corrected for the temperature-independent paramagnetism [$60 \times 10^{-6}$ $cm^3$ $mol^{-1}$ per Cu(II)] and the magnetization of the sample holder.

**Synthesis of 1,3,5,7-tetrakis(tetrazol-5-yl)adamantane trihydrate ($H_4L{\cdot}3H_2O$).** To a mixture of 8.6 g of 1,3,5,7-tetracyanoadamantane[27] and 28.4 g sodium azide in 500 ml of DMF, 39.6 g of anhydrous $ZnCl_2$ was added under stirring. The formed mixture was refluxed for 48 h maintaining anhydrous conditions. Then, 350 ml of DMF was evaporated under reduced pressure and the residue was poured in 800 ml of cold 10% HCl (*caution*: efficient fumehood is required due to evolution of volatile and toxic $HN_3$). The formed precipitate, after ageing for a few hours, was filtered off and washed by water and dried under air at 80 °C until constant weight.

The obtained yellowish crude product (9.9 g) was recrystallized twice from DMSO to yield a pure crystalline $H_4L{\cdot}4DMSO$ adduct. The latter was dissolved in 250 ml of 3% NaOH solution and the product in a hydrate form was recovered by the addition of 50 ml of conc. HCl, filtration and washing with water. The yield of $H_4L{\cdot}3H_2O$ after drying at 80 °C was 9.1 g (54%). The relatively low yield is explained by the use of a crude starting material and losses during recrystallization. $H_4L{\cdot}3H_2O$ is well soluble in DMF and DMSO, sparingly soluble in hot acetic acid and boiling water, but has very low solubility in less polar solvents.

*Caution*: Although $H_4L$ is quite stable under ambient conditions as a hydrate, it is sensitive in dried form at elevated temperatures (>200 °C) and decomposes near-explosively under rapid heating. Sensitization towards explosive decomposition is potentially possible also in the form of complexes/salts with heavy metals. Though the reported coordination compounds are stable, general care should be taken.

$^1H$ NMR (DMSO-$D_6$, 400 MHz): $\delta$ = 2.47 (s, 12H); $^{13}C$ NMR (DMSO-$d_6$, 500 MHz): $\delta$ = 41.7 ($\mathbf{C_{Ad}}H_2$), 34.0 ($\mathbf{C_{Ad}}C_{Tetrazole}$); m.p.: –, instant decomposition was observed at 269 °C (20 K $min^{-1}$ heating rate), IR (KBr): $\nu$, $cm^{-1}$ = 3421 (s), 3130 (m), 3011 (s, br), 2867 (s, br), 2729 (s, br), 2634 (s, br), 1633 (m), 1554 (s), 1456 (w), 1417 (w), 1358 (w), 1254 (s), 1204 (w), 1204 (w), 1108 (w), 1058 (s), 987 (w), 891 (w), 733 (w), 583 (w, br). Elemental analysis, calcd (%) for $C_{14}H_{22}N_{16}O_3$ ($H_4L{\cdot}3H_2O$): C 36.36, H 4.80, N 48.46, found: C 36.61, H 5.12, N 48.74; the water content was independently established by TGA (Fig. S9‡).

**Synthesis of $[Cu_4Cl_4L(DMF)_5]{\cdot}DMF$, 1.** 1.80 g (13.4 mmol) of $CuCl_2$ and 0.90 g (1.95 mmol) of $H_4L{\cdot}3H_2O$ were dissolved in 36 ml of DMF and the solution was sealed in a 50 ml glass flask with a Teflon-lined screw cap. The flask was heated at 70 °C for 14 days. Green octahedral crystals deposited on the bottom of the flask starting from the third day and the process mostly finished in one week. The precipitate was filtered-off under non-strict inert conditions (seconds-long contact with air was allowed), washed with 3 × 2 ml of DMF and dried overnight in a weak stream of inert gas ($N_2$, <0.5 L $h^{-1}$). The yield of the green crystalline product was 0.63 g (26%, ligand based).

The use of anhydrous ligand under the same conditions results in the formation of the same phase. The compound is sparingly soluble in DMF and not soluble in low-polar solvents; it is moderately stable in air for short time, but is sensitive to water vapor and starts to change its color to a greenish-blue after a few hours in open air.

IR (KBr): $\nu$, $cm^{-1}$ = 3436 (s, br), 2930 (w), 2862 (vw), 1651 (vs), 1494 (w), 1461 (m), 1434 (m), 1384 (s, sh), 1250 (w), 1109 (m), 1063 (w), 747 (w), 694 (m), 668 (w); elemental analysis, calcd (%) for $C_{32}H_{54}Cl_4Cu_4N_{22}O_6$: C 31.02, H 4.39, N 24.87, found: C 30.12, H 4.75, N 23.22.

**Synthesis of $[Cd_4Cl_4L(DMF)_7]{\cdot}DMF$, 2.** 940 mg (5.12 mmol) of $CdCl_2$ and 350 mg (0.457 mmol) of $H_4L{\cdot}3H_2O$ were dissolved in 50 ml DMF and sealed in a glass flask with a Teflon-lined screw cap. The flask was heated at 70 °C for 30 days. Transparent octahedral crystals slowly grew on the bottom of the flask and were collected by filtration under non-strict inert-atmosphere after cooling the flask down to RT. After washing with 2 × 2 ml of DMF and drying at RT in a weak inert gas stream overnight, 201 mg (32%) of the product was obtained.

IR (KBr): $\nu$, $cm^{-1}$ = 3436 (s, br), 2931 (w), 2862 (vw), 1658 (vs), 1495 (w), 1458 (m), 1437 (m), 1252 (w), 1104 (m), 1061 (w), 747 (w), 676 (m); elemental analysis, calcd (%) for $C_{35}H_{61}Cl_4Cu_4N_{23}O_7$: C 27.89, H 4.08, N 21.37, found: C 25.70, H 4.37, N 19.92 ($CdCl_2{\cdot}nH_2O$ admixture). The compound is sparingly soluble in DMF and not soluble in low-polar solvents; it is moderately stable in air for minutes, but slowly transforms into other species during hours of contact.

**Synthesis of $[Zn_3Cl_2L(DMF)_4]{\cdot}2DMF$, 3.** 700 mg (5.13 mmol) of $ZnCl_2$ and 350 mg (0.457 mmol) of $H_4L{\cdot}3H_2O$ were dissolved in 50 ml DMF and sealed in a glass flask with a Teflon-lined screw cap. The flask was heated at 70 °C for 30 days. Transparent blocks deposited slowly on the walls of the flask and were collected by filtration under non-strict inert-atmosphere (short contact with air was allowed). The yield of the white crystalline product, after washing with 2 × 3 ml of DMF, quick rinsing with 2 × 3 ml of MeOH and drying in a vacuum, was 130 mg (26%).

IR (KBr): $\nu$, $cm^{-1}$ = 3435 (s, br), 2929 (m), 1659 (vs), 1464 (m), 1437 (m), 1384 (m), 1253 (w), 1203 (w), 1154 (w), 1108 (m), 1064 (w), 774 (w), 748 (w), 686 (w), 668 (w); Elemental analysis, calcd (%) for $C_{32}H_{54}Cl_2N_{22}O_6Zn_3$: C 34.63, H 4.90, N 27.76, found: C 30.28, H 4.85, N 26.55 ($ZnCl_2{\cdot}nH_2O$ admixture). The compound is slightly soluble in DMF and not soluble in low-polar solvents; it is moderately stable in air for minutes.

**Synthesis of $[Mn_2L(DMF)_2(MeOH)_4]{\cdot}DMF{\cdot}2MeOH{\cdot}2H_2O$, 4.** 900 mg (7.14 mmol) of $MnCl_2$ and 450 mg (0.973 mmol) of $H_4L{\cdot}3H_2O$ were dissolved in a mixture of DMF (45 ml) and MeOH (45 ml), and the solution was sealed in a glass flask with a Teflon-lined screw cap. The flask was heated at 70 °C for 9 days. Thin colorless platelet-crystals were formed starting from the third day. The precipitate was filtered off under non-

strict inert conditions, washed by a 3 × 2 ml of DMF–MeOH 1 : 1 mixture and dried overnight in a weak nitrogen stream. The yield of the product consisting of almost colorless thin platelets was 845 mg (87%).

IR (KBr): $\nu$, $cm^{-1}$ = 3425 (s, br), 2935 (m), 1657 (vs), 1498 (w), 1461 (m), 1438 (m), 1384 (s), 1254 (w), 1107 (m), 1061 (m), 743 (m), 676 (m), 412 (vw); elemental analysis, calcd (%) for $C_{29}H_{61}Mn_2N_{19}O_{11}$: C 36.21, H 6.39, N 27.67, found: C 34.26, H 6.30, N 29.91. The compound has appreciable solubility in DMF, but it is not soluble in alcohols and low-polar solvents; it reacts slowly with moist air turning to brown within a few hours of contact.

## Acknowledgements

IB would like to express his sincere gratitude to the Alexander von Humboldt foundation for the postdoctoral fellowship (1135450 STP). The authors thank Dr Igor Baburin for helpful discussions concerning the topology of compounds **1** and **2** and Dr Jana K. Maclaren for collecting the data for the same compounds. We would also like to thank Mr Axel Mundt and Mrs Birgit Tommes for their valuable non-routine help with the analytical equipment. Dr C. Blum and Dr S. Lohmeier from Quantachrome and Dr M. Frenz from Micromeretics are also thanked for their suggestions concerning the conditions of the adsorption measurements and suggestions concerning the nature of the hysteresis observed for compound **1**.

## References

1 G. Aromí, L. A. Barrios, O. Roubeau and P. Gamez, *Coord. Chem. Rev.*, 2011, **255**, 485; J.-P. Zhang, Y.-B. Zhang, J.-B. Lin and X.-M. Chen, *Chem. Rev.*, 2012, **112**, 1001.
2 G. Férey, *Chem. Soc. Rev.*, 2008, **37**, 191–214; S. Kitagawa, R. Kitaura and S. Noro, *Angew. Chem., Int. Ed.*, 2004, **43**, 2334; O. M. Yaghi, M. O'Keeffe, N. W. Ockwig, H. K. Chae, M. Eddaoudi and J. Kim, *Nature*, 2003, **423**, 705.
3 A. U. Czaja, N. Trukhan and U. Müller, *Chem. Soc. Rev.*, 2009, **38**, 1284; S. Ma and H.-C. Zhou, *Chem. Commun.*, 2010, **46**, 44.
4 S. Kitagawa, S. Noro and T. Nakamura, *Chem. Commun.*, 2006, 701.
5 J.-R. Li, R. J. Kuppler and H.-C. Zhou, *Chem. Soc. Rev.*, 2009, **38**, 1477.
6 D. Farrusseng, S. Aguado and C. Pinel, *Angew. Chem., Int. Ed.*, 2009, **48**, 7502.
7 L. J. Murray, M. Dincă and J. R. Long, *Chem. Soc. Rev.*, 2009, **38**, 1294.
8 M. Dinca, A. F. Yu and J. R. Long, *J. Am. Chem. Soc.*, 2006, **128**, 8904.
9 M. Dinca and J. R. Long, *J. Am. Chem. Soc.*, 2007, **129**, 11172.
10 B. Chen, M. Eddaoudi, T. M. Reineke, J. W. Kampf, M. O'Keeffe and O. M. Yaghi, *J. Am. Chem. Soc.*, 2000, **122**, 11559; N. L. Rosi, J. Kim, M. Eddaoudi, B. Chen, M. O'Keeffe and O. M. Yaghi, *J. Am. Chem. Soc.*, 2005, **127**, 1504; J. Kim, B. Chen, T. M. Reineke, H. Li, M. Eddaoudi, D. B. Moler, M. O'Keeffe and O. M. Yaghi, *J. Am. Chem. Soc.*, 2001, **123**, 8239.
11 J. M. Taylor, A. H. Mahmoudkhani and G. K. H. Shimizu, *Angew. Chem., Int. Ed.*, 2007, **46**, 795.
12 D. J. Hoffart, S. A. Dalrymple and G. K. H. Shimizu, *Inorg. Chem.*, 2005, **44**, 8868.
13 D. J. Hoffart, A. P. Cote and G. K. H. Shimizu, *Inorg. Chem.*, 2003, **42**, 8603.
14 T. Muller and S. Bräse, *RSC Adv.*, 2014, **4**, 6886.
15 M. Zhang, Y.-P. Chen and H.-C. Zhou, *CrystEngComm*, 2013, **15**, 9544.
16 M. Dinca, A. Dailly and J. R. Long, *Chemistry*, 2008, **14**, 10280.
17 C. S. Collins, D. Sun, W. Liu, J.-L. Zuo and H.-C. Zhou, *J. Mol. Struct.*, 2008, **890**, 163.
18 I. Boldog, K. V. Domasevitch, J. K. Maclaren, C. Heering, G. Makhloufi and C. Janiak, *CrystEngComm*, 2014, **16**, 148.
19 M. Zhang, Y.-P. Chen, M. Bosch, T. Gentle, K. Wang, D. Feng, Z. U. Wang and H.-C. Zhou, *Angew. Chem., Int. Ed.*, 2014, **53**, 815.
20 I. Boldog, K. V. Domasevitch, I. A. Baburin, H. Ott, B. Gil-Hernandez, J. Sanchiz and C. Janiak, *CrystEngComm*, 2013, **15**, 1235–1243.
21 G. A. Senchyk, A. B. Lysenko, I. Boldog, E. B. Rusanov, A. N. Chernega, H. Krautscheid and K. V. Domasevitch, *Dalton Trans.*, 2012, **41**, 8675.
22 N. B. McKeown and P. M. Budd, *Macromolecules*, 2010, **43**, 5163–5176; R. Dawson, A. I. Cooper and D. J. Adams, *Prog. Polym. Sci.*, 2012, **37**, 530; D. Yuan, W. Lu, D. Zhao and H.-C. Zhou, *Adv. Mater.*, 2011, **23**, 3723; W. Lu, D. Yuan, D. Zhao, C. I. Schilling, O. Plietzsch, T. Muller, S. Bräse, J. Guenther, J. Blümel, R. Krishna, Z. Li and H.-C. Zhou, *Chem. Mater.*, 2010, **22**, 5964.
23 G. R. Newkome and C. Shreiner, *Chem. Rev.*, 2010, **110**, 6338; M. Grillaud, J. Russier and A. Bianco, *J. Am. Chem. Soc.*, 2014, **136**, 810.
24 H. Wang, S. Wang, H. Su, K.-J. Chen, A. L. Armijo, W.-Y. Lin, Y. Wang, J. Sun, K. Kamei, J. Czernin, C. G. Radu and H.-R. Tseng, *Angew. Chem., Int. Ed.*, 2009, **48**, 4344; A. Charlot and R. Auzély-Velty, *Macromolecules*, 2007, **40**, 1147.
25 G. A. Mansoori, P. L. B. Araujo and E. S. Araujo, *Diamondoid Molecules: With Applications in Biomedicine, Materials Science, Nanotechnology and Petroleum Science*, World Scientific, Hackensack, 2012; G. A. Mansoori, T. F. George, L. Assoufid and G. Zhang, *Molecular Building Blocks for Nanotechnology*, Springer, New York, NY, 2007.
26 H. Newman, *Synthesis*, 1972, 692.
27 G. S. Lee, J. N. Bashara, G. Sabih, A. Oganesyan, G. Godjoian, H. M. Duong, E. R. Marinez and C. G. Gutierrez, *Org. Lett.*, 2004, **6**, 1705.
28 H. C. Kolb, M. G. Finn and K. B. Sharpless, *Angew. Chem., Int. Ed.*, 2001, **40**, 2004.

 

29 R.-G. Xiong, X. Xue, H. Zhao, X.-Z. You, B. F. Abrahams and Z. Xue, *Angew. Chem., Int. Ed.*, 2002, **41**, 3800; X.-S. Wang, Y.-Z. Tang, X.-F. Huang, Z.-R. Qu, C.-M. Che, P. W. H. Chan and R.-G. Xiong, *Inorg. Chem.*, 2005, **44**, 5278; R.-G. X. Xue, X.-S. Wang, L.-Z. Wang, R.-G. Xiong, B. F. Abrahams, X.-Z. You, Z.-L. Xue and C.-M. Che, *Inorg. Chem.*, 2002, **41**, 6544.
30 M. H. V. Huynh, M. D. Coburn, T. J. Meyer and M. Wetzler, *Proc. Natl. Acad. Sci. U. S. A.*, 2006, **103**, 10322.
31 F. H. Allen, *Acta Crystallogr., Sect. B: Struct. Sci.*, 2002, **58**, 380. CSD 5.34, Nov. 2012, 3 updates.
32 P. Pachfule and R. Banerjee, *Cryst. Growth Des.*, 2011, **11**, 5176.
33 W. Ouellette and J. Zubieta, *Chem. Commun.*, 2009, 4533.
34 A. W. Addison, T. N. Rao, J. Reedijk, J. van Rijn and G. C. Verschoor, *Dalton Trans.*, 1984, 1349.
35 B. Schmitz, U. Müller, N. Trukhan, M. Schubert, G. Férey and M. Hirscher, *ChemPhysChem*, 2008, **9**, 2181.
36 A. L. Spek, PLATON, *J. Appl. Crystallogr.*, 2003, **36**, 7.
37 T. Düren, F. Millange, G. Férey, K. S. Walton and R. Q. Snurr, *J. Phys. Chem. C*, 2007, **111**, 15350.
38 IUPAC, *Pure Appl. Chem.*, 1982, **54**, 2201.
39 S. S. Mondal, A. Bhunia, I. A. Baburin, C. Jäger, A. Kelling, U. Schilde, G. Seifert, C. Janiak and H.-J. Holdt, *Chem. Commun.*, 2013, **49**, 7567; S. S. Mondal, S. Dey, I. A. Baburin, A. Kelling, U. Schilde, G. Seifert, C. Janiak and H.-J. Holdt, *CrystEngComm*, 2013, **15**, 9394.
40 M. Dinca and J. R. Long, *J. Am. Chem. Soc.*, 2007, **129**, 11172.
41 M. Dinca and J. R. Long, *Angew. Chem., Int. Ed.*, 2008, **47**, 6766.
42 S. Bordiga, L. Regli, F. Bonino, E. Groppo, C. Lamberti, B. Xiao, P. S. Wheatley, R. E. Morris and A. Zecchina, *Phys. Chem. Chem. Phys.*, 2007, **9**, 2676.
43 N. L. Rosi, J. Eckert, M. Eddaoudi, D. T. Vodak, J. Kim, M. O'Keeffe and O. M. Yaghi, *Science*, 2003, **300**, 1127.
44 O. A. Ansón, M. Benham, J. Jagiello, M. A. Callejas, A. M. Benito, W. K. Maser, A. Züttel, P. Sudan and M. T. Martínez, *Nanotechnology*, 2004, **15**, 1503.
45 B. Panella, M. Hirscher and S. Roth, *Carbon*, 2005, **43**, 2209.
46 O. Kahn, *Molecular Magnetism*, VCH, New York, 1993.
47 N. Lah, I. Leban and R. Clérac, *Eur. J. Inorg. Chem.*, 2006, **2006**, 4888.
48 H. A. Habib, J. Sanchiz and C. Janiak, *Inorg. Chim. Acta*, 2009, **362**, 2452.
49 S. Ferrer, P. J. van Koningsbruggen, J. G. Haasnoot, J. Reedijk, H. Kooijman, A. L. Spek, L. Lezama, A. M. Arif and J. S. Miller, *Dalton Trans.*, 1999, 4269.
50 W. Ouellette, A. V. Prosvirin, V. Chieffo, K. R. Dunbar, B. Hudson and J. Zubieta, *Inorg. Chem.*, 2006, **45**, 9346.
51 A. Rodriguez-Dieguez, A. J. Mota, J. Cano, J. Ruiz, D. Choquesillo-Lazarte and E. Colacio, *Dalton Trans.*, 2009, 6335.
52 A. J. Mota, A. Rodriguez-Dieguez, M. A. Palacios, J. M. Herrera, D. Luneau and E. Colacio, *Inorg. Chem.*, 2010, **49**, 8986–8996.
53 A. Burkhardt, E. T. Spielberg and W. Plass, *Inorg. Chem.*, 2008, **47**, 2485.
54 M. Koikawa, H. Yamashita and T. Tokii, *Inorg. Chim. Acta*, 2004, **357**, 2635.
55 A.-Q. Wu, Q.-Y. Chen, M.-F. Wu, F. K. Zheng, F. Chen, G.-C. Guo and J.-S. Huang, *Aust. J. Chem.*, 2009, **62**, 1622.
56 A. Rodríguez-Diéguez, A. J. Mota, J. Cano, J. Ruiz, D. Choquesillo-Lazarte and E. Colacio, *Dalton Trans.*, 2009, 6335.
57 *SAINT*, Data Reduction and Frame Integration Program for the CCD Area-Detector System, Bruker Analytical X-ray Systems, Madison, Wisconsin, USA, 1997–2006; *SADABS: Area-Detector Absorption Correction*, Siemens Industrial Automation, Inc., Madison, Wisconsin, USA, 1996; *XPREP – Data Preparation & Reciprocal Space Exploration, v. 5.1/NT*, Bruker Analytical X-ray Systems, 1997.
58 *CrysAlisPRO*, Oxford Diffraction/Agilent Technologies UK Ltd, Yarnton, England, 2011; *DENZO/SCALEPACK*: Z. Otwinowski and W. Minor, *Methods Enzymol., Macromol. Crystallogr., Part A*, 1997, **276**, 307.
59 SIR: A. Altomare, G. Cascarano, C. Giacovazzo and A. Guagliardi, *J. Appl. Crystallogr.*, 1993, **26**, 343–350. SHELXS: G. M. Sheldrick, *Acta Crystallogr., Sect. A: Fundam. Crystallogr.*, 2008, **64**, 112. SHELXL: *SHELXL-97, Program for refinement of crystal structures*, University of Göttingen, Germany, 1997.
60 V. A. Blatov, *Struct. Chem.*, 2012, **23**, 955–963.
61 E. V. Alexandrov, V. A. Blatov, A. V. Kochetkov and D. M. Proserpio, *CrystEngComm*, 2011, **13**, 3947.
62 U. Mayer, *Pure Appl. Chem.*, 1975, **41**, 291.